Wnt-Dependent Oligodendroglial-Endothelial Interactions Regulate White Matter Vascularization and Attenuate Injury

Manideep Chavali[1, 2, 3], Maria José Ulloa-Navas[4], Pedro Pérez-Borredá[4], Jose Manuel Garcia-Verdugo[4], Patrick S. McQuillen[1], Eric J. Huang[5] and David H. Rowitch[1,2,3,6*]

[1]Department of Pediatrics, UCSF, San Francisco, CA; [2]Eli and Edythe Broad Institute for Stem Cell Research and Regeneration Medicine; [3]New Born Brain Research Institute, UCSF, San Francisco, CA; [4]Laboratorio de Neurobiología Comparada, Instituto Cavanilles, Universidad de Valencia, CIBERNED, TERCEL, Paterna, 46980, Spain. [5]Department of Pathology, UCSF, San Francisco, CA; [6]Department of Paediatrics and Wellcome-MRC Cambridge Stem Cell Institute, University of Cambridge, Hills Road, Cambridge, UK.

Running title: OPC-Endothelial Interactions Regulate White Matter Vasculature

*Correspondence:
David H. Rowitch MD PhD
Department of Paediatrics, University of Cambridge
Hills Road, Cambridge, UK
Tele: +44 01223 769386
E-mail: dhr25@medschl.cam.ac.uk

Summary

Recent studies have indicated oligodendroglial-vascular crosstalk during brain development, but the underlying mechanisms are incompletely understood. We report that oligodendrocyte precursor cells (OPCs) contact sprouting endothelial tip cells in mouse, ferret and human neonatal white matter. Using transgenic mice, we show that increased or decreased OPC density results in cognate changes in white matter vascular investment. Hypoxia promoted both increased OPC numbers and higher white matter vessel density, OPC *WNT7A* expression and endothelial cell expression of the Wnt pathway targets *Apcdd1* and *Axin2*, suggesting paracrine OPC-endothelial signaling. Conditional knockout of OPC *Wntless* resulted in diminished white matter vascular growth in normoxia, while loss of *Wnt7a/b* function blunted the angiogenic response to hypoxia resulting in severe white matter damage. These findings indicate that OPC-endothelial cell interactions regulate neonatal white matter vascular development in a Wnt-dependent manner and further suggest this mechanism is important in attenuating hypoxic injury.

Introduction

Oligodendrocytes are the myelinating cells of the central nervous system. During the process of myelination, developing oligodendrocyte precursors (OPCs) undergo dramatic changes in morphology and size as they differentiate, in some cases achieving a 7000-fold increase in membrane volume, to supply hundreds of myelin segments for nerve axons (Baron and Hoekstra, 2010; Webster, 1971). The consequent bioenergetic-requirements imply that the OPCs must have adequate access to a vascular network for nutrients, oxidative and metabolic substrate during myelination. Indeed, oligodendroglia intimately associate with the developing vasculature (Tsai et al., 2016; Yuen et al., 2014), and blood vessels have been shown to regulate myelination in development and disease (Niu et al., 2019; Rajani et al., 2018; Swire et al., 2019), suggesting bi-directional cell-cell interactions.

In the mammalian brain, angiogenesis commences at embryonic day 9 (E9), when superficial pial blood vessels ingress into the deeper parenchyma (Greenberg and Jin, 2005; Plate, 1999; Vasudevan et al., 2008). By E10, a ventral periventricular plexus forms and starts to branch into the dorsal telencephalon to join the pial vessels (Vasudevan et al., 2008). This network is refined via endothelial cell proliferation, sprouting, branching, vessel regression and stabilization (Carmeliet and Jain, 2011), processes regulated by local secretion of VEGF, BMPs, Wnts and axon guidance cues derived from various neural cell types (Adams and Eichmann, 2010; Carmeliet and Jain, 2011; Eichmann and Thomas, 2013). For example, endothelial β-catenin signaling and neuroepithelial *Wnt7a/b* function has been shown to be essential for embryonic CNS vascular development (Cho et al., 2017a; Daneman et al., 2009; Stenman et al., 2008; Zhou et al., 2014).

The embryonic vasculature undergoes further remodeling in the postnatal and adult stages in a region dependent manner (Bozoyan et al., 2012; Harb et al., 2013). In this context, neuronal reelin regulates cortical vascular organization through activation of endothelial intrinsic Dab/ApoE signaling; disruption in this process results in neuronal positioning errors (Segarra et al., 2018). Adult neurogenesis and angiogenesis have also shown to be coupled in the germinal centers of brain, such as subventricular zone

and subgranular zones (Le Magueresse et al., 2012; Shen et al., 2019; Tavazoie et al., 2008; Wang et al., 2019), where vascular-neural cell crosstalk regulates neuronal progeny generation and migration.

Here we show that OPCs physically interact with angiogenic tip cells in developing white matter and that these interactions are also conserved in mouse, ferret and humans. To understand whether these interactions play a functional role in determining white matter vascular structure, we used mouse transgenic lines to alter OPC numbers *in vivo* and observed a direct impact on white matter vascular density. Neonatal hypoxic injury resulted in white matter angiogenesis in ferret and human brain coupled to increased Wnt target gene expression in white matter endothelial cells. Genetic loss-of-Wnt ligand production in conditional *Wntless* or *Wnt7a/b* transgenic mouse OPCs caused a significant decrease in white matter vascular investment, caused by decrease in sprouting angiogenesis and endothelial proliferation. We also observed that reduced white matter vascular density led to a loss of mature oligodendrocytes and hypomyelination, especially after hypoxic injury. Together, these results show that OPC-endothelial interactions are tightly coupled to ultimate vascular density in forebrain white matter, and that OPC-derived Wnts attenuate susceptibility to hypoxic injury.

Results

Evidence that OPCs physically interact with angiogenic tip cells in white matter. Previous studies have indicated the importance of regional regulation of vascular development, metabolic activity and myelination (Harris and Attwell, 2012; Lam et al., 2010; Paredes et al., 2018). We first investigated the possibility that OPCs physically interact with sprouting endothelial tip cells. As shown (Figure 1A), such physical co-location was apparent through immunohistochemical (IHC) analysis of P1 neonatal mouse brain with markers for OPCs (PDGFRa+Olig2+) and endothelial cells (CD31+); three-dimensional reconstruction showed that OPC processes enwrap the sprouting tip cell filopodia (Figure 1A'). To compare OPC-tip cell proximity versus other glial cell types we used a transgenic *Sox10-GFP* OPC reporter (Kessaris et al., 2006) in conjunction with astroglial (GFAP+) and microglial (Iba1+) markers in P1 white matter. We observed OPCs not only made significantly more frequent physical contacts than other glia, but these contacts were more complex around the tip cell filopodia, as compared to astrocytes and microglial cells (Figure 1B-D; Supplementary Figure 1A).

Further, we found such OPC-endothelial tip cell interactions were conserved in developing ferret and human brain (Figure 1E-F; Supplementary Figure 1B-D). Because angiogenic sprouting continues until the second postnatal week in mouse (Supplementary Figure 1E), we investigated conservation by ultrastructural analysis of human two-year old freshly resected subcortical white matter tissue combined with Olig2 immunogold labelling (Figure 1G). We found that oligodendroglial cell (Olig2 immunogold+) processes formed similar physical contacts with nascent vessels with increased calveolae (Figure 1G-G'). The cell membrane at the OPC-contact site was also characterized by a lack of basement membrane, indicative of tip cell filopodia (Figure 1G'). These results suggest that OPC-endothelial tip cell physical interactions occur during the early neonatal and postnatal white matter development, a period during which active vascular network formation occurs.

Decreased OPC density is associated with white matter hypovascularization. As we observed frequent OPC-endothelial tip cell interactions (Figure 2A), we asked if they

had a functional significance on white matter vascular development. To this end, we intercrossed several lines of transgenic mice to alter OPC numbers in the developing brain. To deplete OPC numbers, we generated *Olig2-cre*, *Sox10-lox-GFP-STOP-lox-DTA* (hereafter called *Sox10-DTA*), a transgenic line in which diphtheria toxin fragment A (DTA) falls under the transcriptional control of the *Sox10* promoter with toxic expression restricted to OPCs (Figure 2B; Supplementary Figure 2A-B) (Kessaris et al., 2006). As shown in Figure 2C-E, we found a ~65% decrease in Olig2+ cell density in white matter and cortical regions of *Sox10-DTA* mice at P1 compared to controls. Interestingly, we observed that white matter vascular network was hypoplastic at this time point (Figure 2C-F).

While *Olig2-Cre* lines targeted up to 75% of OPCs in the neonatal white matter (Supplementary Figure 1A), the cells that escaped Cre targeting subsequently started to repopulate the brain (Supplementary Figure 2C), and by P11 Olig2+ cell numbers had increased by ~15% (Figure 2G-I, Supplementary Figure 2D). We therefore assessed the effect of OPC recovery on white matter vascular development. As shown (Figure 2G-J), although there was a slight increase in Olig2+ cell numbers at P11, the vessel density, length and branching remained significantly lower than controls. Despite this, we did not detect abnormalities in blood brain barrier (BBB) structure/permeability, astrocyte end foot coverage or microglial inflammatory response (Supplementary Figure 2E-H). These findings indicated a positive correlation between white matter oligodendroglial numbers and vascular network density in deep grey and white matter regions (Figure 2K).

Increased oligodendroglial density results in white matter-specific hypervascularization. We next tested if we could promote white matter hypervascularization by bolstering OPC numbers. To achieve this, we intercrossed *Olig2-Cre* and *Braf* $^{V600E\ (fl/+)}$ mice (Dankort et al., 2009) (constitutively active B-Raf; murine sarcoma viral oncogene homolog B, termed *BRAF*^{CA} hereon) (Figure 3A), a mitogenic driver for OPCs (Huillard et al., 2012). Analysis of *BRAF*^{CA} mice at P0 and P9 indicated a significant increase both in Olig2+ cell numbers and vessel density, branching and length in white matter (Figure 3B-I); this phenotype was sustained until P14, the extent of animal survival (Supplementary Figure 3A-C). A recent study showed

that tight perivascular clustering of OPCs on blood vessels in pathological conditions results in BBB damage (Niu et al., 2019). While OPCs in *BRAF*^{CA} mice did cluster on the vessels in the white matter (Figure 3J), we did not observe any disruptions in astrocyte endfeet coverage or BBB damage as assessed by unaltered PLVAP and Glut1/Claudin 5 expression in vessels and more importantly, absence of low molecular weight cadaverine leakage into brain parenchyma (Figure 3K-N; Supplementary Figure 3D). Together, these results indicated that increased OPC numbers directly correlated with density of the white matter vascular network (Figure 3O).

To determine whether OPC density also affected blood vessel coverage in gray matter, we re-analyzed motor and somatosensory cortex from *Sox10-DTA* and *BRAF*^{CA} animals. Although the oligodendroglial cell density was significantly decreased at both P1 and P11 in *Sox10-DTA* cortex, no corresponding decreases in vascular density were noted in these regions (Supplementary Figure 4A-C). Similarly, while oligodendroglial cell density was significantly increased in *BRAF*^{CA} cortex at both P0 and P9, we did not detect any vascular density increase in these regions (Supplementary Figure 4D-F) . These results indicate that oligodendroglial density induced vascular network formation is white matter-specific.

Chronic hypoxic injury acutely increases OPC density and white matter vascular investment in ferret and human neonatal brain. To assess pathophysiological relevance of such OPC-vascular interactions in white matter, we first tested a ferret chronic sublethal hypoxia model (Figure 4A). As shown (Figure 4B), chronic exposure of neonatal kits to mild hypoxia (10% FiO_2) from P10-P20 resulted in hypomyelination consistent with previous reports (Tao et al., 2012). We found that hypoxia caused a significant increase in numbers of immature PDGFRa+Olig2+ OPCs in white matter tracts with reduced numbers of more mature BCAS1+Olig2+ premyelinating cells (Fard et al., 2017) (Figure 4C-D, F). Interestingly, as shown (Figure 4E, F), we also observed a significant increase in vascular density accompanied by higher vessel length and branching in the white matter tracts of hypoxia reared ferret kits.

Human neonatal hypoxic-ischemic encephalopathy (HIE) causes neuronal cell death, gliosis and white matter injury (Supplementary Figure 5A) (Billiards et al., 2008;

Kinney and Back, 1998; Liu and McCullough, 2013; Northington et al., 2011) [26,39]. We analyzed white matter tracts from six cases of HIE and age matched controls (Figure 4G; Supplementary Table 1). Intriguingly, histological analysis of vascular markers showed a significantly increased Col4a+ vessel density and branching in white matter tracts of HIE cases (Figure 4H, I). Furthermore, we also found an increase in immature OPCs (PDGFRa+Olig2+) (Figure 4J, M) and reduced numbers of both premyelinating (BCAS1+Olig2+) and myelinating (Nogo-A+Olig2+) oligodendrocytes in HIE (Figure 4K-M). We found no alterations in vascular junctional marker Claudin 5, indicating vascular integrity (Supplementary Figure 5B). Together, these results suggest that systemic hypoxia-ischemia results in positively correlated acutely increased white matter OPC and vascular densities (Figure 4N).

Endothelial Wnt signaling target gene upregulation in human HIE. Histological analysis of human neonatal brain revealed that OPC proximity to blood vessels coincided with increased expression of the Wnt signaling downstream target Lef1 in endothelial cells (Supplementary Figure 5C). As OPCs make physical contacts with angiogenic vessels and given that Wnts are short range signals that can induce downstream activation in neighboring cells (Figure 4O) (Clevers et al., 2014), we further assessed human HIE cases and controls for evidence of active OPC-driven Wnt signaling in endothelial cells by immunohistochemistry and single molecule fluorescent *in situ* hybridization (smFISH). As shown (Figure 4P, Supplementary Figure 5D-E), we detected that OPCs expressed *WNT7A* mRNA, encoding an angiogenic Wnt, in HIE lesions. We next assessed expression of the Wnt transcriptional targets *Apcdd1* and *Axin2* in CD31+ endothelial cells in HIE lesions and observed a significant increase in their transcripts (Figure 4Q-R). In line with these results, we also observed an increase in Lef1+ endothelial cells in white matter tracts of HIE cases as well as hypoxic ferret brain (Supplementary Figure 5F-H). Together, these findings suggest that Wnt ligand activity in human OPCs results in paracrine activation of Wnt/β-catenin target gene activation in endothelial cells of white matter affected by hypoxic injury.

OPC-encoded *Wntless* function is essential for neonatal white matter vessel development. As increased white matter vascular density in human HIE lesions was coupled with Wnt target gene expression in endothelia, we next asked if OPC-encoded Wnt ligands play a functional role in white matter vascular development *in vivo.* To this end, we generated OPC conditional knockout of *Wntless* (Carpenter et al., 2010), a transmembrane protein required for Wnt family trafficking and secretion (Banziger et al., 2006) (Figure 5A-B). At P3, conditional knockout of *Wntless* in OPCs (hereafter*, Wntless* cKO) did not result in white matter abnormalities (Figure 5C-D); however, by P7 the white matter vascular density started to deteriorate and was significantly reduced by P12 (Figure 5E-J). Oligodendroglial cell numbers remained unaltered at P7 in *Wntless* cKO white matter, but their numbers declined significantly by P12 (Figure 5E-F, H-I). These findings indicated a functional requirement for OPC-derived Wnt cues.

Canonical Wnt signaling is essential for BBB maturation (Daneman et al., 2009; Stenman et al., 2008). To understand if Wnt production from OPCs is needed for BBB integrity, we analyzed small molecular weight cadaverine leakage in normoxic *Wntless* cKO animals; we found no abnormalities in cortex or corpus collosum (Figure 5K-L). Similarly, we did not detect any fibrinogen deposits in brain parenchyma (Figure 5M) or, alterations in expression of the genes, *Plvap, Cldn5, Zic3, Foxf2 and Mfsd2a*, involved in BBB maturation and maintenance in white matter tissue isolates obtained from P8-P10 mice (Figure 5N), or major alterations in the endothelial cell junctional integrity as indicated by PLVAP, Glut1 and Claudin 5 protein expression in white matter vessels (Supplementary Figure 6A). We observed a minor increase in GFAP+ astrocyte reactivity, but not significant changes in activated Iba1+ microglial cell numbers or morphology (Supplementary Figure 6B). These findings indicate that BBB integrity is maintained in *Wntless* cKO animals.

OPC-encoded *Wntless* function is essential for neonatal white matter sprouting angiogenesis and vessel growth. We asked if disruptions in *Wntless* cKO white matter vascular development were the result of deficient neonatal sprouting angiogenesis. We analyzed the developing white matter vessels at P7. As shown (Figure 6A-B), although numbers of sprouting tip cells were unaltered, we observed a

significant decrease in tip cell filopodial length, a finding consistent with previous studies that have shown that decreased angiogenesis is often associated with disruptions in tip cell filopodial development (Fantin et al., 2015).

To understand if the tip cell developmental phenotype was a result of disruptions in known genetic programs, we analyzed candidate tip cell marker and angiokine gene expression in white matter tissue isolates by qPCR. Expression of genes, Vascular endothelial growth factor receptor 2 (*Vegfr2*), Notch ligand and Delta like 4 (*Dll4*) and most other pro-angiogenic cues were unaltered (Figure 6C, D). In contrast, we observed significantly decreased expression of Apelin (*Apln*) (Figure 6C). Apelin expression in endothelial tip cells is known to activate its receptor (APJ) in stalk cells regulating proliferation and vessel growth (del Toro et al., 2010; Kidoya and Takakura, 2012).

To quantify expression of *Apln* at a single cell level we performed smFISH. As shown (Figure 6E-F), *Apln* expression in white matter endothelial tip cells of *Wntless* cKO animals was significantly decreased at P7 and P12 along with *Axin2* (Figure 6F). To further resolve the involvement of canonical Wnt signaling, we quantified Wnt downstream targets *Apcdd1* and *Axin2* in CD31+ endothelial cells and observed a significant decrease in these transcripts (Figure 6G-H). Moreover, we also observed a decline in white matter endothelial cell proliferation in *Wntless* cKO animals. These findings suggest that OPC-specific loss of Wnt ligand production results in down regulation of *Apln* and decreased vessel growth through disrupted sprouting angiogenesis and endothelial cell proliferation (Figure 6I-J).

OPC-encoded *Wntless* is required for white matter integrity. Because we found a decrease in Olig2+ cell numbers in the white matter region of *Wntless* cKO animals, we analyzed if this was due to oligodendroglial cell proliferation defects; however, we found no differences in Olig2+Ki67+ cell numbers at P12 (Supplementary Figure 6C) or alterations in expression of canonical Wnt downstream targets *Axin2* (Figure 7A) or TCF4 (Supplementary Figure 6D). In contrast, we found a significant increase of apoptotic marker cl-caspase 3 in MBP+ oligodendrocytes at P7 in both white matter and deep cortical regions (Figure 7B). At P12, we found significantly decreased numbers of mature CC1+ and *Plp1*+ oligodendrocyte numbers (Figure 7C-F), resulting in white

matter hypomyelination (Figure 7G). We also observed that *Wntless* cKO progressively displayed tremors, ataxia, hind limb clasping and reduced viability after second postnatal week (Supplementary Video 1). Analysis of white matter at P18 (extent of survival) also revealed appearance of axonal damage marker SMI32 and APP+ axonal spheroids (Figure 7H-I). These findings suggest a model in which OPC-encoded *Wntless* function is essential for white matter vascularization, oligodendrocyte survival, postnatal myelination and ultimately white matter integrity.

OPC-encoded *Wnt7a/b* function attenuates white matter injury post-hypoxia. We and others have reported roles for *Wnt7a/b* in regulating embryonic and postnatal CNS developmental angiogenesis (Cho et al., 2017b; Cho et al., 2019; Daneman et al., 2009; Stenman et al., 2008; Yuen et al., 2014; Zhou and Nathans, 2014). To determine whether OPC-encoded *Wnt7a/b* function was essential during development or conferred resilience against hypoxic injury, we generated a compound *Wnt7a/b*-deficient mutant mouse by intercrossing *Olig2-Cre* to conventional *Wnt7a* null and conditional *Wnt7b (fl/fl)* alleles (hereafter *Wnt7dKO*) (Figure 8A), resulting in a significant decrease in *Wnt7* ligand expression in oligodendroglial cells (Figure 8B).

Given that *Wnt7dKO* mice showed improved survival and only subtle developmental impact in white matter versus *Wntless* cKO mice, we tested the effects of superimposed chronic neonatal hypoxemia (Hx) in *Wnt7dKO* mutant mice and controls (Figure 8C). As shown (Figure 8D-E), wildtype mice reared in hypoxic conditions (10% FiO_2; Hx) showed the expected angiogenic response resulting in increased white matter vascular density and branching. In dramatic contrast, this response and endothelial cell proliferation were lacking in hypoxic *Wnt7dKO* mice (Supplementary Figure 7A-B). We confirmed the downregulation of Wnt downstream targets *Apcdd1* and *Axin2* in these mutants (Supplementary Figure 7C-D), and did not observe BBB disruption (absence of PLVAP protein expression changes and no cadaverine leakage) or gliosis in hypoxic *Wnt7dKO* mutants versus controls (Supplementary Figure 7C-G). Of note, *Wnt7a-/-* conventional or *Olig2-Cre/Wnt7b (fl/fl)* conditional single mutants did not show a detectable phenotype post-hypoxic insult

(Supplementary Figure 7H-I). We conclude that combined function of OPC-*Wnt7a/b* is critical for the hypoxia-induced white matter angiogenic response.

As we observed a significant decrease in both oligodendroglial and vessel density in P11 hypoxic reared *Wnt7dKO* mutants (Figure 8D, F), we investigated the timing of this decline. At P7, hypoxic reared *Wnt7dKO* mice began to show vascular density deterioration while oligodendroglial cell density remained unchanged (Supplementary Figure 8A-B). Similar to results above with *Wntless* cKO animals, we observed increased apoptosis in white matter of hypoxic *Wnt7dKO* mutants as well as reduction in CC1+ and *Plp1*+ mature oligodendrocytes, severe hypomyelination, increased expression of axonal damage marker SMI32 and reduced white matter volume (Figure 8G-M). In contrast to white matter, cortical oligodendroglial and OPC numbers remained unchanged (Supplementary Figure 8D-E). Together, these findings indicate that OPC-encoded *Wnt7* function is a critical determinant of white matter susceptibility to hypoxic injury. They do not exclude roles for other OPC-encoded Wnt ligands or other OPC-derived angiogenic factors in regulation of developmental white matter angiogenesis in normoxic or hypoxic conditions.

Discussion

Here we addressed the fundamental question of how vascular density is orchestrated in mammalian cortical white matter and implications of this for resilience against hypoxic insult in neonatal brain. A major insight is that OPC-endothelial tip cell interactions play a direct role in this process and that alterations in OPC density and angiogenic signaling drive vascular remodeling in white matter. We show that oligodendroglial-endothelial cell interactions attenuate susceptibility to hypoxic neonatal brain injury in a Wnt-dependent manner, a finding with implications for human neonatal white matter injury, cerebral palsy and white matter stroke. These and other findings discussed below indicate bi-directional crosstalk between OPCs and vasculature during development and in disease.

Evidence for OPC-endothelial bi-directional crosstalk in white matter. Vascular investment of primordial brain regions depends on neuroepithelial and radial glial angiogenic cues including canonical Wnt signaling (Grutzendler et al., 2014; Lam et al., 2010; Ma et al., 2013; Stenman et al., 2008). The embryonic vasculature is subsequently remodeled at neonatal stages by neuronal and glial populations (Bozoyan et al., 2012; Harb et al., 2013; Ma et al., 2013; Paredes et al., 2018; Segarra et al., 2018; Vasudevan et al., 2008), including NG2 glia (Minocha et al., 2015). Several studies show that OPC-encoded *HIF* function regulates white matter angiogenesis via paracrine signaling as well as cell-autonomous OPC maturation and myelination (Allan et al., 2020; Yuen et al., 2014). Here we extend insights into this process and show the OPCs and blood vessels engage in further cell-cell interactions in neonatal brain. Strikingly, we found that OPCs form what appear by ultrastructure to be direct and frequent contacts with sprouting endothelial tip cells during white matter development. Our data showed tight coupling of OPC number and white matter angiogenesis in transgenic mouse lines with decreased or increased OPC numbers. Together, these findings firmly establish that OPCs are major regulators of white matter angiogenesis.

Embryonic OPCs depend on the vasculature for distribution throughout the CNS (Tsai et al., 2016), indicating that bi-directional cross-talk is essential during development. Moreover, during remyelination clustering of OPCs along blood vessels in

MS white matter lesions has been observed (Niu et al., 2019) and a recent study elucidated the role for endothelial cells in adaptive myelination (Swire et al., 2019). Other lines of evidence indicate this relationship persists postnatally until adult stages. For example, oligodendrocyte-vascular crosstalk has been shown to regulate the BBB maintenance, and myelination (Niu et al., 2019; Rajani et al., 2018; Swire et al., 2019) and vascular dysfunction (e.g., in chronic hypertension) underlies white matter abnormalities in various pathological settings (Montagne et al., 2018; Rajani and Williams, 2017). Further research is warranted to investigate the complex inter-relationships between the oligodendroglial lineage and the vasculature during development and in neurological diseases.

OPC-encoded Wnt signaling is essential for neonatal white matter angiogenesis and axonal, but not BBB, integrity *in vivo*. Angiogenesis in mouse brain is robust from E9.5 until second postnatal week (Paredes et al., 2018). Although the role of embryonic Wnt signaling and radial glia in regulation of CNS vasculature is known (Cho et al., 2017b; Cho et al., 2019; Daneman et al., 2009; Stenman et al., 2008; Zhou and Nathans, 2014), postnatal angiogenic roles for Wnt signaling in OPCs are incompletely understood. Here we incapacitated all Wnt ligand production by conditionally targeting *Wntless* with *Olig1-cre*, which drives activity in OPCs (Silbereis et al., 2014). Interestingly, while OPC number was unaffected in white matter of P7 *Wntless* mutants, we found a severe impact on tip cell development and blood vessel density, indicating that OPC-encoded Wnt activity is essential for neonatal angiogenesis. Oligodendroglia also express *Wnt 3, 4, 6, 9a* and *10a* (Zhang et al., 2014). In contrast to normoxic *Olig1-cre/Wntless* mice, *Olig2-cre, Wnt7dKO* had a mild phenotype without impact on the developing vasculature. Because *Wntless* function is required for all Wnt ligands, these findings suggest that other Wnts beside Wnt7 compensate for loss of *Wnt7a/b* during normal neonatal white matter angiogenesis.

In contrast, specific roles for *Wnt7* were indicated in the setting of hypoxic injury. We found that chronic hypoxia in mouse and ferret as well as human HIE cases, showed significantly increased OPC and vessel density in white matter tracts coupled with an increase in canonical Wnt/β-catenin targets Lef1, *Apcdd1*and *Axin2*) in

endothelial cells. In human HIE lesions, we observed *WNT7A*-expressing OPCs. Additionally, *Wnt7a/b* mutants in the hypoxic setting showed dramatic abrogation of vessel induction post-hypoxia and severe damage to white matter and hypomyelination, suggesting specific roles for OPC-encoded *Wnt7* function to maintain resilience against hypoxic injury.

Canonical Wnt signaling in CNS endothelial cells is required for BBB maturation in a region-restricted manner (Cho et al., 2017b; Wang et al., 2018; Wang et al., 2012; Zhou and Nathans, 2014; Zhou et al., 2014); for instance, loss-of-*Frizzled 4* function results in BBB disruptions only in cerebellum, retina and olfactory bulb (Wang et al., 2012). We found that neither alterations in OPC density or deletion of OPC-encoded Wnt ligand activity resulted in BBB disruption. This indicates that OPC-Wnt activity acts primarily to support endothelial tip cell development and vessel growth, but not BBB integrity.

OPC-Wnt is a primary angiogenic signal that acts in a paracrine manner in neonatal white matter. Autocrine Wnt signaling inhibits of OPC differentiation (Fancy et al., 2009; Fancy et al., 2014; Fancy et al., 2011; Hammond et al., 2015). However, in both *Wntless* and *Wnt7dKO* mutants, we found that expression of the Wnt downstream target *Axin2* was unaltered within OPCs themselves nor did we observe precocious OPC differentiation; thus, we found no evidence for autocrine effects. Wnt ligands act as short range signals (Clevers et al., 2014) and have specific roles in brain angiogenesis (Vanhollebeke et al., 2015). We found that loss-of-OPC Wnt function in both *Wntless* and *Wnt7dKO* animals resulted in decreased white matter vessel density and down-regulation of canonical Wnt/β-catenin targets *Apcdd1* and *Axin2* in endothelial cells, indicating cell-to-cell signaling. Moreover, OPC-Wnt signaling was specifically required to maintain expression of *Apelin* in angiogenic tip cells in contrast to expression of the pro-angiogenic cues *Vegfa, Ndp, Sema3E* and *Ntn1* and other tip cell genes (*Vegfr2* and *Dll4*) in *Wntless* mutants. Because OPCs form intimate contacts with endothelial tip cells, these findings collectively indicate OPC-Wnt acts in a paracrine manner to regulate white vascular development.

Therapeutic implications. OPCs have been shown to react to –and be targeted in –a wide spectrum of injuries including neonatal HIE (Billiards et al., 2008; Fancy et al., 2011), stroke (Chen et al., 2018; Joseph et al., 2016) and multiple sclerosis (Fancy et al., 2011), pathologies associated with chronic hypomyelination. As angiogenesis is a fundamental initial response to a variety of tissue insults, the OPC-vascular crosstalk we describe here might also be adaptive because they can migrate rapidly along blood vessels into brain lesions (Niu et al., 2019). Our data suggest a new role for OPCs in this context, namely, directly regulating angiogenesis in the setting of CNS white matter lesion repair. As several studies have shown abnormal OPC Wnt signaling in human neonatal while matter injury and MS (Fancy et al., 2009; Fancy et al., 2014), an implication of this study is that post-injury angiogenic wound healing could be compromised.

White matter ischemic stroke is a leading cause of motor dysfunction and cognitive impairment (Roman et al., 2002), and studies in experimental models have shown that OPC numbers are upregulated during the recovery phase of the injury (Joseph et al., 2016; Sozmen et al., 2016; Zhang et al., 2011); indeed, OPC neuroprotection during the acute phase of stroke injury improves functional recovery (Chen et al., 2018). Interestingly, OPCs have been suggested to play a beneficial role in recovery by promoting post injury angiogenesis and BBB rescue in various stroke injury models (Kishida et al., 2019; Wang et al., 2020). As to the nature of secreted pro-angiogenic cues, the current study indicates a specific function for OPC-encoded *Wnt7.*

Members of the vascular endothelial growth factor (VEGF) family are well-established hypoxic signaling targets (Himmels et al., 2017) that show developmental expression within OPCs (Cahoy et al., 2008). Indeed, VEGF expression has also been reported to be regulated by canonical Wnt signaling (Easwaran et al., 2003; Wu et al., 2015). Similarly, other pro-angiogenic candidate factors such as semaphorins and neuropilins are also expressed by oligodendroglial lineage cells. Because, aged patients show diminished recovery from stroke compared to young adults (Bousser, 2012; Ovbiagele and Nguyen-Huynh, 2011), and OPC functions decline in aged animals (Ruckh et al., 2012), a related question is how OPC angiogenic factor production is regulated over the life course? Future work is needed to investigate OPC-encoded

regulators of blood vessel development over the life course and their functional relevance in neonatal, juvenile and/or adult white matter injuries.

Figure Legends

Figure 1: Oligodendroglial Precursors Interact with Endothelial Tip Cells in Developing White Matter Tracts of Mouse, Ferret and Human Brain
(A-A') OPC-Endothelial tip cell interactions in P1 mouse forebrain coronal section (A). OPCs (PDGFRa+Olig2+ cells) in white matter frequently contact endothelial tip cell (CD31+) filopodia (A'). Isosurface reconstruction shows that OPC processes enwrap the tip cell filopodia (indicated by white arrowheads). Scale bars: 25μm.
(B) Representative images from a P1 *Sox10-GFP* transgenic mouse, labelled with GFAP and CD31 markers showing tip cell filopodia being enwrapped by OPC (Sox10-GFP positive cells) processes and astroglial (GFAP+ cells) processes. Isosurface reconstructions reveal that OPCs processes form complex and frequent contacts with the tip cell filopodia compared to astroglial cell processes (indicated by white arrowheads). Scale bar: 20μm
(C) Representative image of a tip cell being contacted by only OPCs but not astroglial cells (indicated by magenta arrowhead). Scale bar: 20μm
(D) Quantification of tip cells contacted by OPCs and astroglial cells or both in the P1 white matter.
(E-E') OPC-Endothelial tip cell interactions in P10 ferret brain coronal section (E). OPCs in white matter tracts frequently contact and enwrap endothelial tip cell filopodia (E') (indicated by white arrowheads in isosurface reconstruction). Scale bars: 25μm.
(F-F') OPC-Endothelial tip cell interactions in 17 gestational weeks (GW) human brain coronal section (F). OPCs in developing deep cortical regions adjacent to the ventricle, frequently contact endothelial tip cell filopodia (F'). Isosurface reconstruction reveals OPC processes enwrapping the tip cell filopodia (indicated by white arrowheads). Scale bars: 25μm.
(G-G') Persistent oligodendroglial-tip cell interactions in early postnatal human brain revealed by ultrastructural analysis of subcortical white matter resection from 2-year-old human brain, combined with Olig2 immunogold labelling (G). High magnification images show oligodendroglial cell process (puesdocolored-green; indicated by black arrowhead) contacting filopodial extensions from a nascent vessel (puesdocolor-red) with calveolae (indicated by black arrows) (G'). Scale bars: 5μm (G), 500nm (G'). BV: Blood Vessel, RBC: Red Blood Cell: O: Oligodendroglial Cell. For all quantifications data are shown as mean $\pm$ S.D. and are analyzed by a two-tailed unpaired Student's t test. n=3 animals. Significance between two groups are shown as *p<0.05, **p<0.01.

Figure 2: **Oligodendroglial Cell Ablation Leads to Developmental Hypovascularization of White Matter in *Sox10-DTA* Transgenic Mice**
(A) Cartoon illustration of neural and glial cell types interacting with developing vas-culature in the postnatal forebrain.
(B) Schematic of genetic strategy for *Sox10-DTA* transgenic mouse generation.
(C) Representative images of P1 - Control (CTRL) and *Sox10-DTA* mouse coronal brain sections labelled with CD31 showing significant decrease in white matter vessel density. Scale bar: 100μm
(D) High magnification images of cingulum region (highlighted areas from (C)), showing Sox10-GFP+Olig2+ oligodendroglial cells and CD31+ blood vessels. Scale bar: 50μm

(E) Illustration of regions of white matter analyzed along the rostro-caudal axis.
(E') Quantification of Olig2+ cells in the P1 white matter.
(F) Quantification of P1 white matter blood vessel coverage, branching and length.
(G) Coronal sections from P11- Control (CTRL) and *Sox10-DTA* mouse brains labelled with CD31 showing significant decrease in white matter vessel density. Scale bar: 100μm
(H) High magnification images of cingulum region (highlighted areas from (G)), showing Sox10-GFP+Olig2+ oligodendroglial cells and CD31+ blood vessels Scale bar: 50μm.
(I) Quantification of Olig2+ cells in the P11 white matter.
(J) Quantification of P11 white matter blood vessel coverage, branching and length.
(K) White matter oligodendroglial cell density and vessel coverage are positively correlated. For all quantifications data are shown as mean ± S.D. and are analyzed by a two-tailed unpaired Student's t test. n=6 animals/genotype for (E'-F) and n=5 for (I-K). Significance between two groups are shown as *p<0.05, **p<0.01, **** p<0.0001.

Figure 3: Increased Oligodendroglial Density Induces Hypervascularization of Developing White Matter in *BRAF^{CA}* Transgenic Mice
(A) Schematic of genetic strategy for *BRAF^{CA}* transgenic mouse generation.
(B) DAPI-stained coronal sections from P0 - Control (CTRL) and *BRAF^{CA}* mutant mouse brains. *BRAF^{CA}* mutants do not show any defects in cortical or white matter cytoarchitecture. Scale bar: 100μm
(C) High magnification images of cingulum region (highlighted areas from (B)), showing increased Olig2+ oligodendroglial cells and CD31+ blood vessel coverage. Scale bar: 50μm
(D) Quantification of white matter Olig2+ cells in the P0 mice.
(E) Quantification of white matter blood vessel coverage, branching and length in P0 mice.
(F) Forebrain regions in *BRAF^{CA}* mice appears normal and do not show any neoplasms at P9. DAPI-stained coronal sections from CTRL and BRAF^{CA} brains. Scale bar: 100μm
(G) High magnification images of highlighted areas from (C), showing sustained increase in Olig2+ oligodendroglial cells and CD31+ blood vessel coverage. Scale bar: 50μm.
(H) Quantification of white matter Olig2+ cells in P9 mice.
(I) Quantification of white matter blood vessel coverage, branching and length in P9 mice.
(J) PDGFRa+ OPCs form clusters on CD31+ blood vessels in BRAF^{CA} mutant white matter. Bottom panel shows an isosurface rendering of the same image. Scale bar: 20μm.
(K) Representative images of white matter region labelled with GFAP, Aquaporin 4 (AQP4) and Collagen 4a (Col4a) in CTRL and BRAF^{CA} mice. Note that no astrocyte endfeet coverage abnormalities were observed. Scale bar: 50μm.
(L) Representative images of white matter region from CTRL and BRAF^{CA} brain sections labelled with Claudin 5 and Plasmalemma vesicle protein (PLVAP). Note the absence of Claudin 5 negative and PLVAP positive vessels in white matter, indicating no blood brain barrier (BBB) damage. Inset in top panel shows choroid plexus vessels from the

same section showing PLVAP expression confirming successful PLVAP labelling. Scale bar: 50μm.
(M) Representative images of white matter regions from P9 CTRL and $BRAF^{CA}$ mice injected with low molecular weight cadaverine tracer injection. Scale bar: 50μm.
(N) Cadaverine-555 intensity quantifications in CTRL and $BRAF^{CA}$ brain sections shows no significant changes, indicating no tracer leakage into brain parenchyma in $BRAF^{CA}$ mutants.
(O) White matter oligodendroglial cell density and vascular coverage are positively correlated. For all quantifications data are shown as mean ± S.D. and are analyzed by a two-tailed unpaired Student's t test. n=5 animals/genotype for data presented in (D-I, O), n=3 animals/genotype for data presented in (N). Significance between two groups are shown as *p<0.05, **p<0.01, ***p<0.001, **** p<0.0001.

Figure 4: Oligodendroglial Precursor Induced White Matter Vascular Density Increases in Neonatal White Matter Injury is Wnt7 Dependent
(A) Schematic and cartoon illustration of ferret chronic sub-lethal hypoxic injury paradigm.
(B) Chronic hypoxia causes hypomyelination in ferret brain. Coronal brain sections from Normoxic (Nx) and Hypoxic (Hx) reared ferret kits stained with myelin basic protein (MBP). Scale bar: 500μm.
(C-D) Increase in PDGFRa+Olig2 oligodendroglial precursors (C) and decrease in immature BCAS1+Olig2+ immature oligodendrocytes (D). Scale bars: 25μm.
(E) Increased CD31+ blood vessel coverage in white matter tracts of ferrets reared in hypoxia. Scale bar: 25μm.
(F) Quantification of oligodendroglial lineage cells and blood vessel coverage, branching and length in white matter tracts of normoxic and hypoxic ferrets at P20.
(G) Cartoon illustration of human hypoxic ischemic encephalopathy (HIE) white matter tracts.
(H) Representative images of white matter tracts of cingulate from human cases of hypoxic ischemic encephalopathy (HIE) and age matched controls immunostained with blood vessel marker Collagen 4a (Col4a). Note a robust increase in vascular coverage in HIE. Scale bar: 50μm.
(I) Quantification of vessel coverage and branching in white matter tracts of Control (CTRL) and HIE cases.
(J-M) Increase in oligodendroglial precursor (PDGFRa+Olig2+) cell numbers (J, M) and decrease in mature oligodendrocyte cell numbers; BCAS1+Olig2+ (K,M) and Nogo-A+Olig2+MBP+ (L,M) in white matter tracts of human HIE cases revealed by immunohistochemical analysis. Scale bars: 25μm.
(N) Cartoon illustration of hypoxia induced cellular changes in the white matter tracts.
(O) Cartoon illustration of OPC induced endothelial intrinsic Wnt signaling.
(P) Multiplex smFISH labelling of *PDGFRa* and *Wnt7a* in control and HIE cases. Scale bar: 10μm.
(Q) Multiplex smFISH of Wnt signaling downstream targets *Apcdd1* and *Axin2* combined with CD31 immunolabelling reveals an increase in endothelial cell Wnt signaling in white matter tracts of HIE cases. Scale bar: 10μm.

(R) Quantification of *Apcdd1* and *Axin2* RNA spots in CD31+ endothelial cell nuclei. For all quantifications data are shown as mean ± S.D. and are analyzed by a two-tailed unpaired Student's t test. n=3 animals/condition for data represented in (F), n=6 cases/condition for data represented in (I) and (M) and n=3 cases/condition for data represented in (R). Each data point represents a single case in (R), overlaying violin plots represent RNAspots quantified from atleast 100 cells from 3 different control and HIE cases. Significance between two groups are shown as *p<0.05, **p<0.01.

Figure 5: Oligodendroglial Intrinsic Wnt ligand Activity is Crucial for Postnatal White Matter Vascular Development.

(A) Wnt ligands are activated by Wntless in the endoplasmic reticulum and are then transported to the plasma membrane, where they are secreted and bind to Wnt receptors.

(B) Schematic of genetic strategy for *Wntless conditional knockout (Wntless* cKO*)* mouse generation.

(C) White matter development in *Wntless cKO* is not affected at P3. Representative images from P3 cortical white matter showing Olig2+ oligodendroglial cells and CD31+ blood vessels. Scale bar: 50μm.

(D) Quantification of white matter Olig2+ cell numbers and CD31+ vessel coverage.

(E) Representative images from P7 cortical white matter region showing Olig2+ oligodendroglial cells and CD31+ blood vessels. Note a decrease in blood vessel density compared to control. Scale bar: 50μm.

(F-G) Quantification of P7 white matter Olig2+ cell numbers, vessel coverage, branching and length.

(H) Representative images from P12 cortical white matter showing significantly reduced Olig2+ oligodendroglial cells and CD31+ blood vessel coverage in *Wntless* cKO*.* Scale bar: 50μm.

(I-J) Quantification of P12 white matter Olig2+ cell numbers, vessel coverage, branching and length.

(K) Representative images from cortex (top panels) and corpus collosum (bottom panels) regions of Cadaverine-555 injected P10 mice reveal no tracer leakage indicating no BBB disruptions in *Wntless* mutants.

(L) Quantification of Cadaverine-555 fluorescence intensity in cortex and corpus collosum regions from control and *Wntless* cKO animals.

(M) Representative images of corpus collosum region from control and *Wntless* cKO mice labelled with Glut1 and Fibrinogen. Note absence of fibrinogen deposits in *Wntless* cKO mice indicating no BBB damage. Bottom left panel shows positive control for fibrinogen staining from cerebellum of Norrin ($NDP^{-/Y}$) mutants.

(N) Gene expression analysis by qPCR of white matter tissue isolates from control and *Wntless* cKO reveals no alterations in expression of genes involved in BBB maturation and maintenance. For all quantifications data are shown as mean ± S.D. and are analyzed by a two-tailed unpaired Student's t test. n=4 animals/genotype for data shown in (D), n=6 for (F-G), n=5 for (I-J), n=3 for (L) and n=6 for (N). Significance between two groups are shown as *p<0.05, ***p<0.001, **** p<0.0001.

Figure 6: Oligodendroglial Intrinsic Wnt Ligand Activity is Required for White Matter Tip Cell Development and Vessel Growth.
(A) Representative images of white matter vessels labelled with CD31 from P7 control and *Wntless* cKO animals show angiogenic tip cells (indicated by arrowheads). High magnification images of boxed region reveal a decrease in tip cell development and isosurface reconstruction shows a decrease in tip cell filopodial length. Scale bars: 25μm.
(B) Quantification of tip cells and length of tip cell filopodia in white matter vessels.
(C) Gene expression analysis of white matter tissue isolates by qPCR from control and *Wntless* cKO animals reveals decrease in expression of tip cell gene *Apelin (Apln)*.
(D) Gene expression analysis of white matter tissue isolates by qPCR from control and *Wntless* cKO animals show no alterations in expression of pro-angiogenic genes involved tip cell development.
(E) smFISH combined with CD31 immunolabelling reveals a decrease in expression of tip cell gene *Apln in Wntless* cKO white matter endothelial cells. Scale bar: 5μm.
(F) Multiplex smFISH of *Apln* and *Axin2* combined with CD31 immunolabelling shows reduced Wnt signaling in white matter endothelial tip cells. Scale bar: 5μm.
(G) Multiplex smFISH of Wnt signaling downstream targets *Apcdd1* and *Axin2* combined with CD31 immunolabelling reveals a decrease in endothelial cell intrinsic Wnt signaling in *Wntless* cKO white matter. Scale bar: 5μm.
(H) Quantification of *Apcdd1* and *Axin2* RNA spots in CD31+ endothelial cell nuclei.
(M) Immunolabelling of ERG (endothelial cell nuclei marker) and Ki67 (proliferation marker) in P12 white matter regions reveal decrease in white matter endothelial cell proliferation in *Wntless* cKO animals. Scale bar: 50μm
(N) Quantification of ERG+ and Ki67+ cells in white matter. For all quantifications data are shown as mean $\pm$ S.D. and are analyzed by a two-tailed unpaired Student's t test. n=3 animals/genotype for data shown in (B), n=6 for (C-D), n=3 for (H), n=5 for (J). Significance between two groups are shown as *p<0.05, **p<0.01.

Figure 7: Disruption in Oligodendroglial Intrinsic Wnt ligand Activity Results in Loss of Mature Oligodendrocytes and Hypomyelination.
(A) Multiplex smFISH of *Plp1, PDGFRa* and *Axin2* show no alterations in oligodendroglial intrinsic canonical Wnt/β-catenin activity in *Wntless* cKO animals. *PDGFRa*+ OPCs are outlined in white. Scale Bar: 5μm.
(B) Cortical white matter regions labelled with MBP and Cleaved Caspase 3 show increase in oligodendrocyte apoptosis in white matter and deep cortex regions in *Wntless c*KO animals at P7. Insets show highlighted regions. Scale bar: 100μm and 50μm for insets. Right panel shows quantification of Cleaved Caspase 3+ cells in white matter.
(C-D) Significant loss of mature oligodendrocytes (CC1+Olig2+ cells) in *Wntless* cKO animals at P12. Scale bar: 50μm.
(E-F) Significant reduction in mature oligodendrocytes expressing *Plp1* mRNA in *Wntless cKO* at P12. Scale bar: 50μm.
(G) Hypomyelination of *Wntless* cKO animals at P12 revealed by myelin basic protein (MBP) and pan-neurofilament marker (NF) immunostaining. Scale bar: 50μm.

(H) Increase in expression of axonal damage marker SMI32 in the corpus collosum of *Wntless* cKO animals at P18. Scale bar: 10μm.
(I) Appearance of amyloid precursor protein (APP+) axonal spheroids in P18 *Wntless* cKO aniamls (indicated by black arrowheads), indicating axon damage; corpus callosum and external capsule regions are shown. Scale bar: 10μm. For all quantifications data are shown as mean ± S.D. and are analyzed by a two-tailed unpaired Student's t test. n=6 animals/genotype for data represented in (B) and n=5 and 4 each for data represented in (D) and (F) respectively. Significance between two groups are shown as **p<0.01, ***p<0.001.

Figure 8: OPC-encoded *Wnt7* Function is Critical for Post Injury Angiogenesis, Myelination and White Matter Integrity.
(A) Schematic of *Wnt7a/b* double knockout mouse *(Wnt7dKO)* generation strategy.
(B) Immunostaining of Wnt7a/b in brain sections at P7 from control and *Wnt7dKO* animals show downregulation of Wnt7 ligand expression in Olig2+ oligodendroglial cells. Scale bar: 10μm.
(C) Schematic of mouse chronic sub-lethal hypoxic injury paradigm.
(D) Representative images of Olig2+ oligodendroglial cells and CD31+ blood vessels from P11 cortical white matter region from normoxic and hypoxic reared control and *Wnt7dKO* animals. Note a significant decrease in blood vessel coverage and oligodendroglial cell numbers in hypoxic *Wnt7dKO* animals compared to control. Scale bar: 50μm.
(E) Quantification of blood vessel coverage and branching at P11.
(F) Quantification of Olig2+ cell numbers in white matter at P11.
(G-H) Loss of CC1+Olig2+ mature oligodendroglial cells in white matter region of hypoxic *Wnt7dKO* animals compared to control. Scale bar: 25μm.
(I-J) Significant decline in mature oligodendrocytes expressing *Plp1* mRNA (and MBP protein, inset) in hypoxic *Wnt7dKO* mutants at P11. Scale bars represent 50 μm for (I) and 100 μm for images in insets.
(K) Axonal damage revealed by SMI32 and NF immunostaining in the corpus collosum of hypoxic *Wnt7dKO* animals. Scale bar: 10μm.
(L) Decrease in corpus collosum thickness and axonal myelination in hypoxic *Wnt7dKO* mutants at P11 revealed by MBP and NF immunostaining. Scale bar: 50μm.
(M) Quantification of corpus collosum thickness. For all quantifications data are shown as mean ± S.D. and are analyzed by a two-tailed unpaired Student's t test. n=7 animals per genotype and condition for data represented in (D-F, M), n=5 for (H) and n=4 for (J). Significance between two groups are shown as *p<0.05, ***p<0.001, **** p<0.0001.

References

1. Adams, R.H., and Eichmann, A. (2010). Axon guidance molecules in vascular patterning. Cold Spring Harb Perspect Biol *2*, a001875.
2. Allan, K.C., Hu, L.R., Morton, A.R., Scavuzzo, M.A., Gevorgyan, A.S., Clayton, B.L.L., Bederman, I.R., Hung, S., Bartels, C.F., Madhavan, M.*, et al.* (2020). Non-Canonical Targets of HIF1a Drive Cell-Type-Specific Dysfunction. bioRxiv, 2020.2004.2003.003632.
3. Banziger, C., Soldini, D., Schutt, C., Zipperlen, P., Hausmann, G., and Basler, K. (2006). Wntless, a conserved membrane protein dedicated to the secretion of Wnt proteins from signaling cells. Cell *125*, 509-522.
4. Baron, W., and Hoekstra, D. (2010). On the biogenesis of myelin membranes: sorting, trafficking and cell polarity. FEBS Lett *584*, 1760-1770.
5. Billiards, S.S., Haynes, R.L., Folkerth, R.D., Borenstein, N.S., Trachtenberg, F.L., Rowitch, D.H., Ligon, K.L., Volpe, J.J., and Kinney, H.C. (2008). Myelin abnormalities without oligodendrocyte loss in periventricular leukomalacia. Brain Pathol *18*, 153-163.
6. Bousser, M.G. (2012). Stroke prevention: an update. Front Med *6*, 22-34.
7. Bozoyan, L., Khlghatyan, J., and Saghatelyan, A. (2012). Astrocytes control the development of the migration-promoting vasculature scaffold in the postnatal brain via VEGF signaling. J Neurosci *32*, 1687-1704.
8. Cahoy, J.D., Emery, B., Kaushal, A., Foo, L.C., Zamanian, J.L., Christopherson, K.S., Xing, Y., Lubischer, J.L., Krieg, P.A., Krupenko, S.A.*, et al.* (2008). A transcriptome database for astrocytes, neurons, and oligodendrocytes: a new resource for understanding brain development and function. J Neurosci *28*, 264-278.
9. Carmeliet, P., and Jain, R.K. (2011). Molecular mechanisms and clinical applications of angiogenesis. Nature *473*, 298-307.
10. Carpenter, A.C., Rao, S., Wells, J.M., Campbell, K., and Lang, R.A. (2010). Generation of mice with a conditional null allele for Wntless. Genesis *48*, 554-558.
11. Chen, Y., Zhang, L., Yu, H., Song, K., Shi, J., Chen, L., and Cheng, J. (2018). Necrostatin-1 Improves Long-term Functional Recovery Through Protecting Oligodendrocyte Precursor Cells After Transient Focal Cerebral Ischemia in Mice. Neuroscience *371*, 229-241.
12. Cho, C., Smallwood, P.M., and Nathans, J. (2017a). Reck and Gpr124 Are Essential Receptor Cofactors for Wnt7a/Wnt7b-Specific Signaling in Mammalian CNS Angiogenesis and Blood-Brain Barrier Regulation. Neuron *95*, 1221-1225.
13. Cho, C., Smallwood, P.M., and Nathans, J. (2017b). Reck and Gpr124 Are Essential Receptor Cofactors for Wnt7a/Wnt7b-Specific Signaling in Mammalian CNS Angiogenesis and Blood-Brain Barrier Regulation. Neuron *95*, 1056-1073 e1055.
14. Cho, C., Wang, Y., Smallwood, P.M., Williams, J., and Nathans, J. (2019). Molecular determinants in Frizzled, Reck, and Wnt7a for ligand-specific signaling in neurovascular development. Elife *8*.

15. Clevers, H., Loh, K.M., and Nusse, R. (2014). Stem cell signaling. An integral program for tissue renewal and regeneration: Wnt signaling and stem cell control. Science *346*, 1248012.
16. Daneman, R., Agalliu, D., Zhou, L., Kuhnert, F., Kuo, C.J., and Barres, B.A. (2009). Wnt/beta-catenin signaling is required for CNS, but not non-CNS, angiogenesis. Proc Natl Acad Sci U S A *106*, 641-646.
17. Dankort, D., Curley, D.P., Cartlidge, R.A., Nelson, B., Karnezis, A.N., Damsky, W.E., Jr., You, M.J., DePinho, R.A., McMahon, M., and Bosenberg, M. (2009). Braf(V600E) cooperates with Pten loss to induce metastatic melanoma. Nat Genet *41*, 544-552.
18. del Toro, R., Prahst, C., Mathivet, T., Siegfried, G., Kaminker, J.S., Larrivee, B., Breant, C., Duarte, A., Takakura, N., Fukamizu, A.*, et al.* (2010). Identification and functional analysis of endothelial tip cell-enriched genes. Blood *116*, 4025-4033.
19. Easwaran, V., Lee, S.H., Inge, L., Guo, L., Goldbeck, C., Garrett, E., Wiesmann, M., Garcia, P.D., Fuller, J.H., Chan, V.*, et al.* (2003). beta-Catenin regulates vascular endothelial growth factor expression in colon cancer. Cancer Res *63*, 3145-3153.
20. Eichmann, A., and Thomas, J.L. (2013). Molecular parallels between neural and vascular development. Cold Spring Harb Perspect Med *3*, a006551.
21. Fancy, S.P., Baranzini, S.E., Zhao, C., Yuk, D.I., Irvine, K.A., Kaing, S., Sanai, N., Franklin, R.J., and Rowitch, D.H. (2009). Dysregulation of the Wnt pathway inhibits timely myelination and remyelination in the mammalian CNS. Genes Dev *23*, 1571-1585.
22. Fancy, S.P., Harrington, E.P., Baranzini, S.E., Silbereis, J.C., Shiow, L.R., Yuen, T.J., Huang, E.J., Lomvardas, S., and Rowitch, D.H. (2014). Parallel states of pathological Wnt signaling in neonatal brain injury and colon cancer. Nat Neurosci *17*, 506-512.
23. Fancy, S.P., Harrington, E.P., Yuen, T.J., Silbereis, J.C., Zhao, C., Baranzini, S.E., Bruce, C.C., Otero, J.J., Huang, E.J., Nusse, R.*, et al.* (2011). Axin2 as regulatory and therapeutic target in newborn brain injury and remyelination. Nat Neurosci *14*, 1009-1016.
24. Fantin, A., Lampropoulou, A., Gestri, G., Raimondi, C., Senatore, V., Zachary, I., and Ruhrberg, C. (2015). NRP1 Regulates CDC42 Activation to Promote Filopodia Formation in Endothelial Tip Cells. Cell Rep *11*, 1577-1590.
25. Fard, M.K., van der Meer, F., Sanchez, P., Cantuti-Castelvetri, L., Mandad, S., Jakel, S., Fornasiero, E.F., Schmitt, S., Ehrlich, M., Starost, L.*, et al.* (2017). BCAS1 expression defines a population of early myelinating oligodendrocytes in multiple sclerosis lesions. Sci Transl Med *9*.
26. Greenberg, D.A., and Jin, K. (2005). From angiogenesis to neuropathology. Nature *438*, 954-959.
27. Grutzendler, J., Murikinati, S., Hiner, B., Ji, L., Lam, C.K., Yoo, T., Gupta, S., Hafler, B.P., Adelman, R.A., Yuan, P.*, et al.* (2014). Angiophagy prevents early embolus washout but recanalizes microvessels through embolus extravasation. Sci Transl Med *6*, 226ra231.

28. Hammond, E., Lang, J., Maeda, Y., Pleasure, D., Angus-Hill, M., Xu, J., Horiuchi, M., Deng, W., and Guo, F. (2015). The Wnt effector transcription factor 7-like 2 positively regulates oligodendrocyte differentiation in a manner independent of Wnt/beta-catenin signaling. J Neurosci *35*, 5007-5022.
29. Harb, R., Whiteus, C., Freitas, C., and Grutzendler, J. (2013). In vivo imaging of cerebral microvascular plasticity from birth to death. J Cereb Blood Flow Metab *33*, 146-156.
30. Harris, J.J., and Attwell, D. (2012). The energetics of CNS white matter. J Neurosci *32*, 356-371.
31. Himmels, P., Paredes, I., Adler, H., Karakatsani, A., Luck, R., Marti, H.H., Ermakova, O., Rempel, E., Stoeckli, E.T., and Ruiz de Almodovar, C. (2017). Motor neurons control blood vessel patterning in the developing spinal cord. Nat Commun *8*, 14583.
32. Huillard, E., Hashizume, R., Phillips, J.J., Griveau, A., Ihrie, R.A., Aoki, Y., Nicolaides, T., Perry, A., Waldman, T., McMahon, M.*, et al.* (2012). Cooperative interactions of BRAFV600E kinase and CDKN2A locus deficiency in pediatric malignant astrocytoma as a basis for rational therapy. Proc Natl Acad Sci U S A *109*, 8710-8715.
33. Joseph, M.J., Caliaperumal, J., and Schlichter, L.C. (2016). After Intracerebral Hemorrhage, Oligodendrocyte Precursors Proliferate and Differentiate Inside White-Matter Tracts in the Rat Striatum. Transl Stroke Res *7*, 192-208.
34. Kessaris, N., Fogarty, M., Iannarelli, P., Grist, M., Wegner, M., and Richardson, W.D. (2006). Competing waves of oligodendrocytes in the forebrain and postnatal elimination of an embryonic lineage. Nat Neurosci *9*, 173-179.
35. Kidoya, H., and Takakura, N. (2012). Biology of the apelin-APJ axis in vascular formation. J Biochem *152*, 125-131.
36. Kinney, H.C., and Back, S.A. (1998). Human oligodendroglial development: relationship to periventricular leukomalacia. Semin Pediatr Neurol *5*, 180-189.
37. Kishida, N., Maki, T., Takagi, Y., Yasuda, K., Kinoshita, H., Ayaki, T., Noro, T., Kinoshita, Y., Ono, Y., Kataoka, H.*, et al.* (2019). Role of Perivascular Oligodendrocyte Precursor Cells in Angiogenesis After Brain Ischemia. J Am Heart Assoc *8*, e011824.
38. Lam, C.K., Yoo, T., Hiner, B., Liu, Z., and Grutzendler, J. (2010). Embolus extravasation is an alternative mechanism for cerebral microvascular recanalization. Nature *465*, 478-482.
39. Le Magueresse, C., Alfonso, J., Bark, C., Eliava, M., Khrulev, S., and Monyer, H. (2012). Subventricular zone-derived neuroblasts use vasculature as a scaffold to migrate radially to the cortex in neonatal mice. Cereb Cortex *22*, 2285-2296.
40. Liu, F., and McCullough, L.D. (2013). Inflammatory responses in hypoxic ischemic encephalopathy. Acta Pharmacol Sin *34*, 1121-1130.
41. Ma, S., Kwon, H.J., Johng, H., Zang, K., and Huang, Z. (2013). Radial glial neural progenitors regulate nascent brain vascular network stabilization via inhibition of Wnt signaling. PLoS Biol *11*, e1001469.
42. Minocha, S., Valloton, D., Brunet, I., Eichmann, A., Hornung, J.P., and Lebrand, C. (2015). NG2 glia are required for vessel network formation during embryonic development. Elife *4*.

43. Montagne, A., Nikolakopoulou, A.M., Zhao, Z., Sagare, A.P., Si, G., Lazic, D., Barnes, S.R., Daianu, M., Ramanathan, A., Go, A.*, et al.* (2018). Pericyte degeneration causes white matter dysfunction in the mouse central nervous system. Nat Med *24*, 326-337.
44. Niu, J., Tsai, H.H., Hoi, K.K., Huang, N., Yu, G., Kim, K., Baranzini, S.E., Xiao, L., Chan, J.R., and Fancy, S.P.J. (2019). Aberrant oligodendroglial-vascular interactions disrupt the blood-brain barrier, triggering CNS inflammation. Nat Neurosci *22*, 709-718.
45. Northington, F.J., Chavez-Valdez, R., and Martin, L.J. (2011). Neuronal cell death in neonatal hypoxia-ischemia. Ann Neurol *69*, 743-758.
46. Ovbiagele, B., and Nguyen-Huynh, M.N. (2011). Stroke epidemiology: advancing our understanding of disease mechanism and therapy. Neurotherapeutics *8*, 319-329.
47. Paredes, I., Himmels, P., and Ruiz de Almodovar, C. (2018). Neurovascular Communication during CNS Development. Dev Cell *45*, 10-32.
48. Plate, K.H. (1999). Mechanisms of angiogenesis in the brain. J Neuropathol Exp Neurol *58*, 313-320.
49. Rajani, R.M., Quick, S., Ruigrok, S.R., Graham, D., Harris, S.E., Verhaaren, B.F.J., Fornage, M., Seshadri, S., Atanur, S.S., Dominiczak, A.F.*, et al.* (2018). Reversal of endothelial dysfunction reduces white matter vulnerability in cerebral small vessel disease in rats. Sci Transl Med *10*.
50. Rajani, R.M., and Williams, A. (2017). Endothelial cell-oligodendrocyte interactions in small vessel disease and aging. Clin Sci (Lond) *131*, 369-379.
51. Roman, G.C., Erkinjuntti, T., Wallin, A., Pantoni, L., and Chui, H.C. (2002). Subcortical ischaemic vascular dementia. Lancet Neurol *1*, 426-436.
52. Ruckh, J.M., Zhao, J.W., Shadrach, J.L., van Wijngaarden, P., Rao, T.N., Wagers, A.J., and Franklin, R.J. (2012). Rejuvenation of regeneration in the aging central nervous system. Cell Stem Cell *10*, 96-103.
53. Segarra, M., Aburto, M.R., Cop, F., Llao-Cid, C., Hartl, R., Damm, M., Bethani, I., Parrilla, M., Husainie, D., Schanzer, A.*, et al.* (2018). Endothelial Dab1 signaling orchestrates neuro-glia-vessel communication in the central nervous system. Science *361*.
54. Shen, J., Wang, D., Wang, X., Gupta, S., Ayloo, B., Wu, S., Prasad, P., Xiong, Q., Xia, J., and Ge, S. (2019). Neurovascular Coupling in the Dentate Gyrus Regulates Adult Hippocampal Neurogenesis. Neuron *103*, 878-890 e873.
55. Silbereis, J.C., Nobuta, H., Tsai, H.H., Heine, V.M., McKinsey, G.L., Meijer, D.H., Howard, M.A., Petryniak, M.A., Potter, G.B., Alberta, J.A.*, et al.* (2014). Olig1 function is required to repress dlx1/2 and interneuron production in Mammalian brain. Neuron *81*, 574-587.
56. Sozmen, E.G., Rosenzweig, S., Llorente, I.L., DiTullio, D.J., Machnicki, M., Vinters, H.V., Havton, L.A., Giger, R.J., Hinman, J.D., and Carmichael, S.T. (2016). Nogo receptor blockade overcomes remyelination failure after white matter stroke and stimulates functional recovery in aged mice. Proc Natl Acad Sci U S A *113*, E8453-E8462.

57. Stenman, J.M., Rajagopal, J., Carroll, T.J., Ishibashi, M., McMahon, J., and McMahon, A.P. (2008). Canonical Wnt signaling regulates organ-specific assembly and differentiation of CNS vasculature. Science *322*, 1247-1250.
58. Swire, M., Kotelevtsev, Y., Webb, D.J., Lyons, D.A., and Ffrench-Constant, C. (2019). Endothelin signalling mediates experience-dependent myelination in the CNS. Elife *8*.
59. Tao, J.D., Barnette, A.R., Griffith, J.L., Neil, J.J., and Inder, T.E. (2012). Histopathologic correlation with diffusion tensor imaging after chronic hypoxia in the immature ferret. Pediatr Res *71*, 192-198.
60. Tavazoie, M., Van der Veken, L., Silva-Vargas, V., Louissaint, M., Colonna, L., Zaidi, B., Garcia-Verdugo, J.M., and Doetsch, F. (2008). A specialized vascular niche for adult neural stem cells. Cell Stem Cell *3*, 279-288.
61. Tsai, H.H., Niu, J., Munji, R., Davalos, D., Chang, J., Zhang, H., Tien, A.C., Kuo, C.J., Chan, J.R., Daneman, R.*, et al.* (2016). Oligodendrocyte precursors migrate along vasculature in the developing nervous system. Science *351*, 379-384.
62. Vanhollebeke, B., Stone, O.A., Bostaille, N., Cho, C., Zhou, Y., Maquet, E., Gauquier, A., Cabochette, P., Fukuhara, S., Mochizuki, N.*, et al.* (2015). Tip cell-specific requirement for an atypical Gpr124- and Reck-dependent Wnt/beta-catenin pathway during brain angiogenesis. Elife *4*.
63. Vasudevan, A., Long, J.E., Crandall, J.E., Rubenstein, J.L., and Bhide, P.G. (2008). Compartment-specific transcription factors orchestrate angiogenesis gradients in the embryonic brain. Nat Neurosci *11*, 429-439.
64. Wang, J., Cui, Y., Yu, Z., Wang, W., Cheng, X., Ji, W., Guo, S., Zhou, Q., Wu, N., Chen, Y.*, et al.* (2019). Brain Endothelial Cells Maintain Lactate Homeostasis and Control Adult Hippocampal Neurogenesis. Cell Stem Cell *25*, 754-767 e759.
65. Wang, L., Geng, J., Qu, M., Yuan, F., Wang, Y., Pan, J., Li, Y., Ma, Y., Zhou, P., Zhang, Z.*, et al.* (2020). Oligodendrocyte precursor cells transplantation protects blood-brain barrier in a mouse model of brain ischemia via Wnt/beta-catenin signaling. Cell Death Dis *11*, 9.
66. Wang, Y., Cho, C., Williams, J., Smallwood, P.M., Zhang, C., Junge, H.J., and Nathans, J. (2018). Interplay of the Norrin and Wnt7a/Wnt7b signaling systems in blood-brain barrier and blood-retina barrier development and maintenance. Proc Natl Acad Sci U S A *115*, E11827-E11836.
67. Wang, Y., Rattner, A., Zhou, Y., Williams, J., Smallwood, P.M., and Nathans, J. (2012). Norrin/Frizzled4 signaling in retinal vascular development and blood brain barrier plasticity. Cell *151*, 1332-1344.
68. Webster, H.D. (1971). The geometry of peripheral myelin sheaths during their formation and growth in rat sciatic nerves. J Cell Biol *48*, 348-367.
69. Wu, C., Chen, J., Chen, C., Wang, W., Wen, L., Gao, K., Chen, X., Xiong, S., Zhao, H., and Li, S. (2015). Wnt/beta-catenin coupled with HIF-1alpha/VEGF signaling pathways involved in galangin neurovascular unit protection from focal cerebral ischemia. Sci Rep *5*, 16151.
70. Yuen, T.J., Silbereis, J.C., Griveau, A., Chang, S.M., Daneman, R., Fancy, S.P.J., Zahed, H., Maltepe, E., and Rowitch, D.H. (2014). Oligodendrocyte-encoded HIF function couples postnatal myelination and white matter angiogenesis. Cell *158*, 383-396.

71. Zhang, R.L., Chopp, M., Roberts, C., Jia, L., Wei, M., Lu, M., Wang, X., Pourabdollah, S., and Zhang, Z.G. (2011). Ascl1 lineage cells contribute to ischemia-induced neurogenesis and oligodendrogenesis. J Cereb Blood Flow Metab *31*, 614-625.
72. Zhang, Y., Chen, K., Sloan, S.A., Bennett, M.L., Scholze, A.R., O'Keeffe, S., Phatnani, H.P., Guarnieri, P., Caneda, C., Ruderisch, N.*, et al.* (2014). An RNA-sequencing transcriptome and splicing database of glia, neurons, and vascular cells of the cerebral cortex. J Neurosci *34*, 11929-11947.
73. Zhou, Y., and Nathans, J. (2014). Gpr124 controls CNS angiogenesis and blood-brain barrier integrity by promoting ligand-specific canonical wnt signaling. Dev Cell *31*, 248-256.
74. Zhou, Y., Wang, Y., Tischfield, M., Williams, J., Smallwood, P.M., Rattner, A., Taketo, M.M., and Nathans, J. (2014). Canonical WNT signaling components in vascular development and barrier formation. J Clin Invest *124*, 3825-3846.

Acknowledgements

We would like to thank members of the Rowitch lab for their valuable suggestions and technical assistance with experimental setup. J.M.G.V and M.J.U.N would like to acknowledge Patricia García-Tárraga and Ana Saurí-Tamarit for their assistance with electron microscopy experiments. We would also like to thank Sasha Mikhailova for assistance with ferret hypoxia experiments. M.C. acknowledges fellowship awards from the American Heart Association and The Children's Heart Foundation and funding support from a Career Development Grant awarded by Cerebral Palsy Alliance Research Foundation. J.M.G.V is funded by Red deTerapia Celular (TerCel-RD16/0011/0026) and the Valencian Council for Innovation, Universities Science and Digital Society (PROMETEO/2019/075). M.J.U.N was supported by a McDonald Fellowship from the Multiple Sclerosis International Federation. This work was supported by funding from the National Multiple Sclerosis Foundation (to D.H.R.), the Adelson Medical Research Foundation (D.H.R), the European Research Council (D.H.R.) and the National Institutes of Health, NINDS (1K99NS117804 to M.C; P01-NS083513 to D.H.R., E.J.H and P.S.M).

Author Contributions

M.C. and D.H.R. conceived the original idea. M.C. performed all experiments and data analysis. M.J.U.N. and J.M.G.V. performed Olig2 immunogold labelling and electron microscopy studies. P.S.M and E.J.H provided advice on experimental design related to ferret hypoxic injury and human HIE experiments respectively. M.C. and D.H.R. designed all experiments and wrote the manuscript.

Supplementary Materials

Materials and Methods
Reagent and Resource Table
Supplementary Tables 1 and 2
Supplementary Figures S1-S8.
Supplementary Video 1

Figure 1

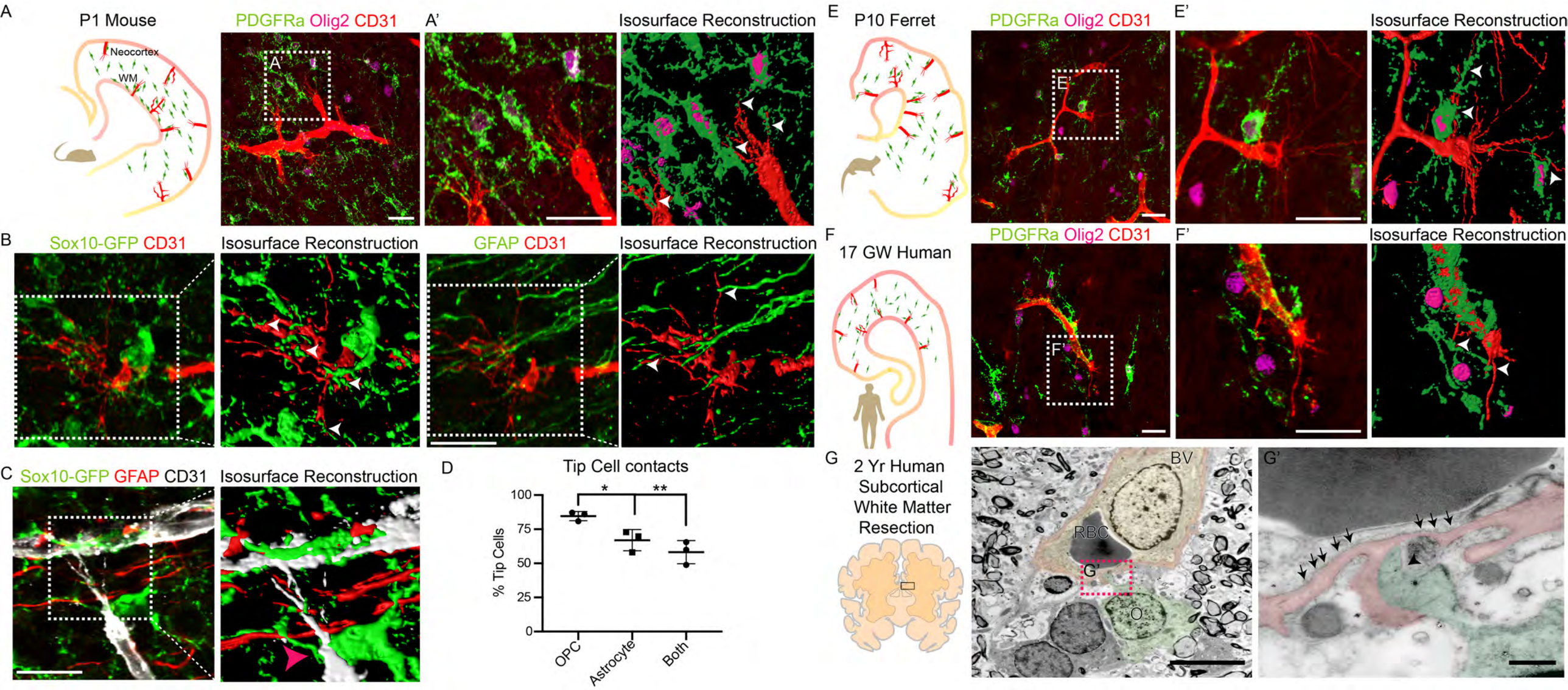
A
P1 Mouse
Neocortex
WM
PDGFRa Olig2 CD31
A'
Isosurface Reconstruction
B
Sox10-GFP CD31
Isosurface Reconstruction
GFAP CD31
Isosurface Reconstruction
C
Sox10-GFP GFAP CD31
Isosurface Reconstruction
D
Tip Cell contacts
% Tip Cells
100
75
50
25
0
*
**
OPC
Astrocyte
Both
E
P10 Ferret
PDGFRa Olig2 CD31
E'
Isosurface Reconstruction
F
17 GW Human
PDGFRa Olig2 CD31
F'
Isosurface Reconstruction
G
2 Yr Human
Subcortical
White Matter
Resection
BV
RBC
G'
O
G'

Figure 2

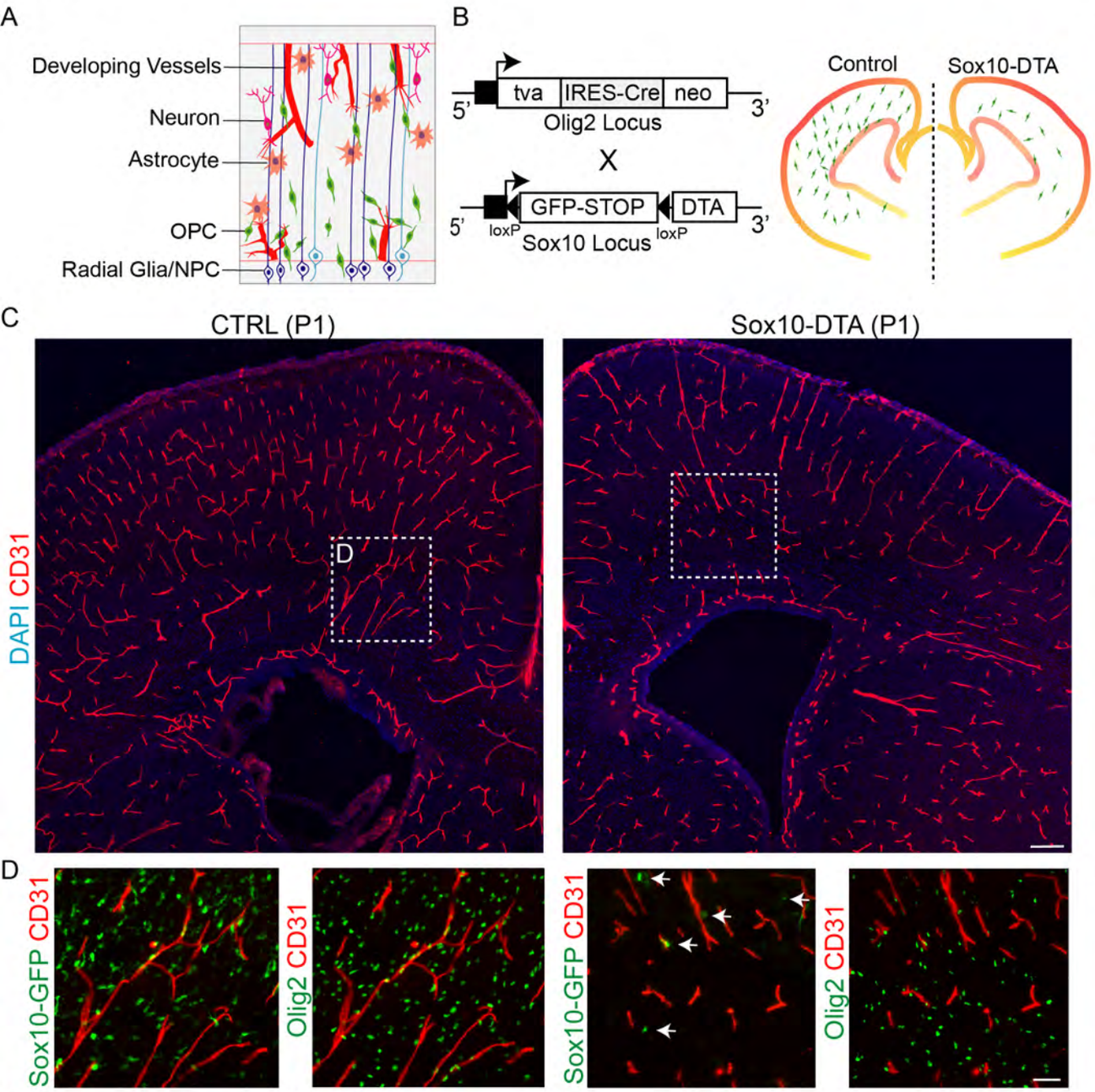
A
Developing Vessels
Neuron
Astrocyte
OPC
Radial Glia/NPC
B
tva
IRES-Cre
neo
5'
3'
Olig2 Locus
X
GFP-STOP
DTA
loxP
Sox10 Locus
loxP
Control
Sox10-DTA
C
CTRL (P1)
Sox10-DTA (P1)
DAPI CD31
D
G
CTRL (P11)
Sox10-DTA (P11)
H
D
Sox10-GFP CD31
Olig2 CD31
H
E
E'
F
I
J
K
Olig2+ Cells (P1)
% Vessel Coverage (P1)
Number of Branches (P1)
Total Vessel Length in mm (P1)
Olig2+ Cells (P11)
% Vessel Coverage (P11)
Number of Branches (P11)
Total Vessel Length in mm (P11)
CTRL
Sox10-DTA
p = 0.0363
r = 0.6640

Figure 3

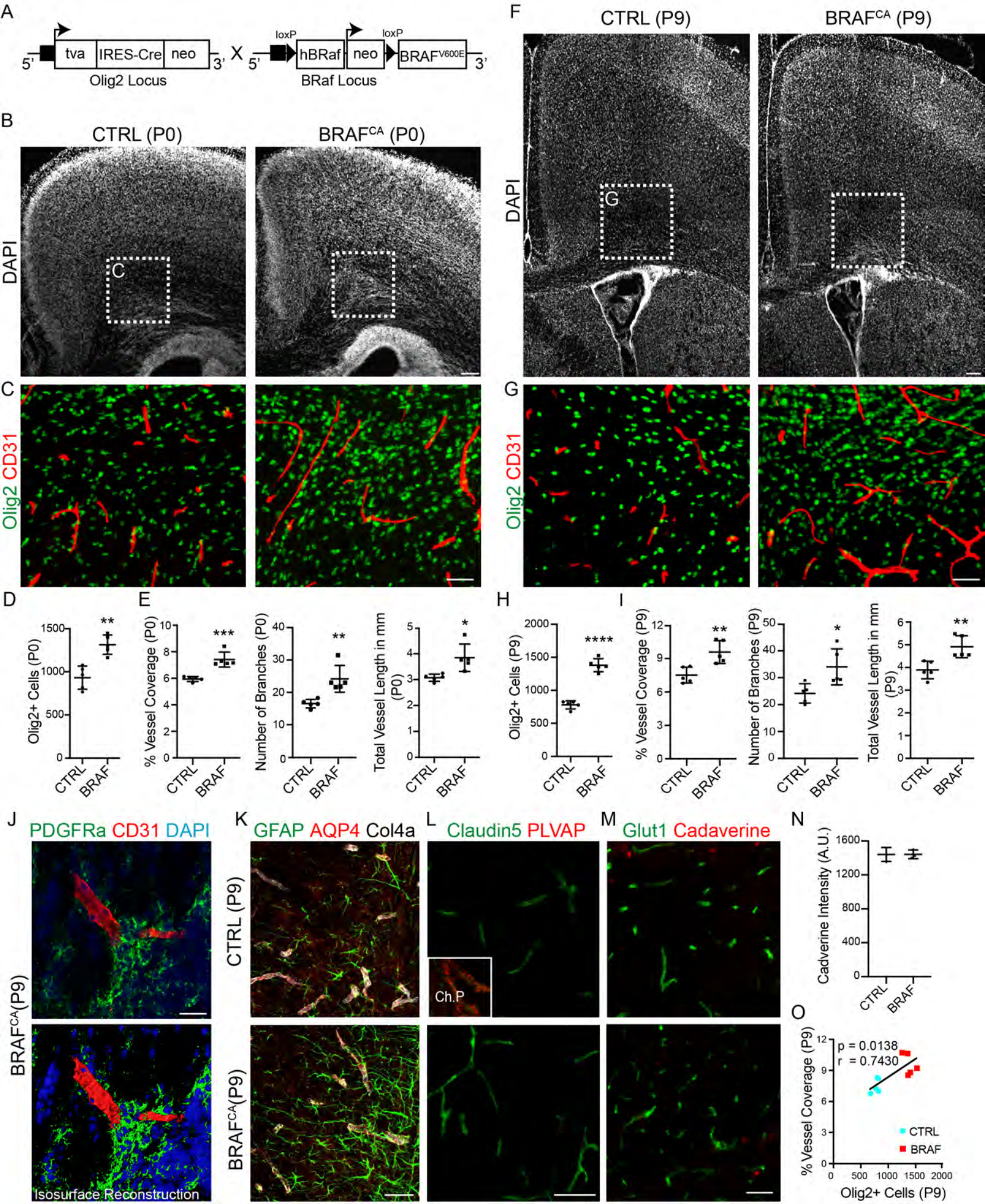
A
5'
tva
IRES-Cre
neo
3'
X
Olig2 Locus
loxP
hBRaf
neo
loxP
BRAF V600E
BRaf Locus
B
CTRL (P0)
BRAF CA (P0)
DAPI
C
Olig2 CD31
F
CTRL (P9)
BRAF CA (P9)
G
D
Olig2+ Cells (P0)
E
% Vessel Coverage (P0)
Number of Branches (P0)
Total Vessel Length in mm (P0)
H
Olig2+ Cells (P9)
I
% Vessel Coverage (P9)
Number of Branches (P9)
Total Vessel Length in mm (P9)
CTRL
BRAF
J
PDGFRa CD31 DAPI
BRAF CA (P9)
Isosurface Reconstruction
K
GFAP AQP4 Col4a
CTRL (P9)
L
Claudin5 PLVAP
Ch.P
M
Glut1 Cadaverine
N
Cadaverine Intensity (A.U.)
O
p = 0.0138
r = 0.7430
% Vessel Coverage (P9)
Olig2+ Cells (P9)

Figure 4

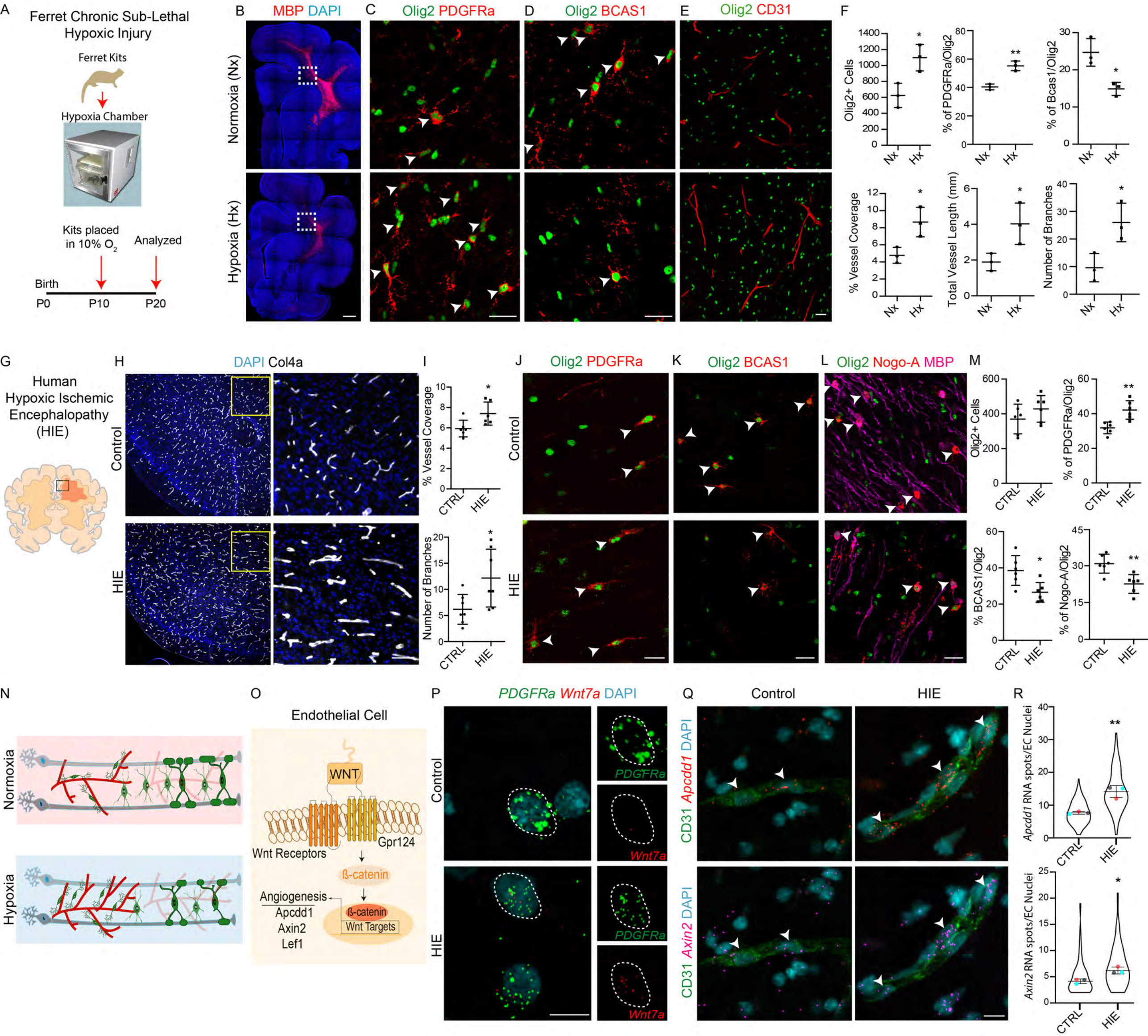
A
Ferret Chronic Sub-Lethal Hypoxic Injury
Ferret Kits
Hypoxia Chamber
Kits placed in 10% O2
Analyzed
Birth
P0
P10
P20
B
MBP DAPI
C
Olig2 PDGFRa
D
Olig2 BCAS1
E
Olig2 CD31
Normoxia (Nx)
Hypoxia (Hx)
F
Olig2+ Cells
% of PDGFRa/Olig2
% of Bcas1/Olig2
% Vessel Coverage
Total Vessel Length (mm)
Number of Branches
Nx
Hx
G
Human Hypoxic Ischemic Encephalopathy (HIE)
H
DAPI Col4a
Control
HIE
I
% Vessel Coverage
Number of Branches
CTRL
HIE
J
Olig2 PDGFRa
K
Olig2 BCAS1
L
Olig2 Nogo-A MBP
M
Olig2+ Cells
% of PDGFRa/Olig2
% BCAS1/Olig2
% of Nogo-A/Olig2
N
Normoxia
Hypoxia
O
Endothelial Cell
WNT
Gpr124
Wnt Receptors
ß-catenin
Angiogenesis
Apcdd1
Axin2
Lef1
Wnt Targets
P
PDGFRa Wnt7a DAPI
Q
Control
HIE
CD31 Apcdd1 DAPI
CD31 Axin2 DAPI
R
Apcdd1 RNA spots/EC Nuclei
Axin2 RNA spots/EC Nuclei

Figure 5

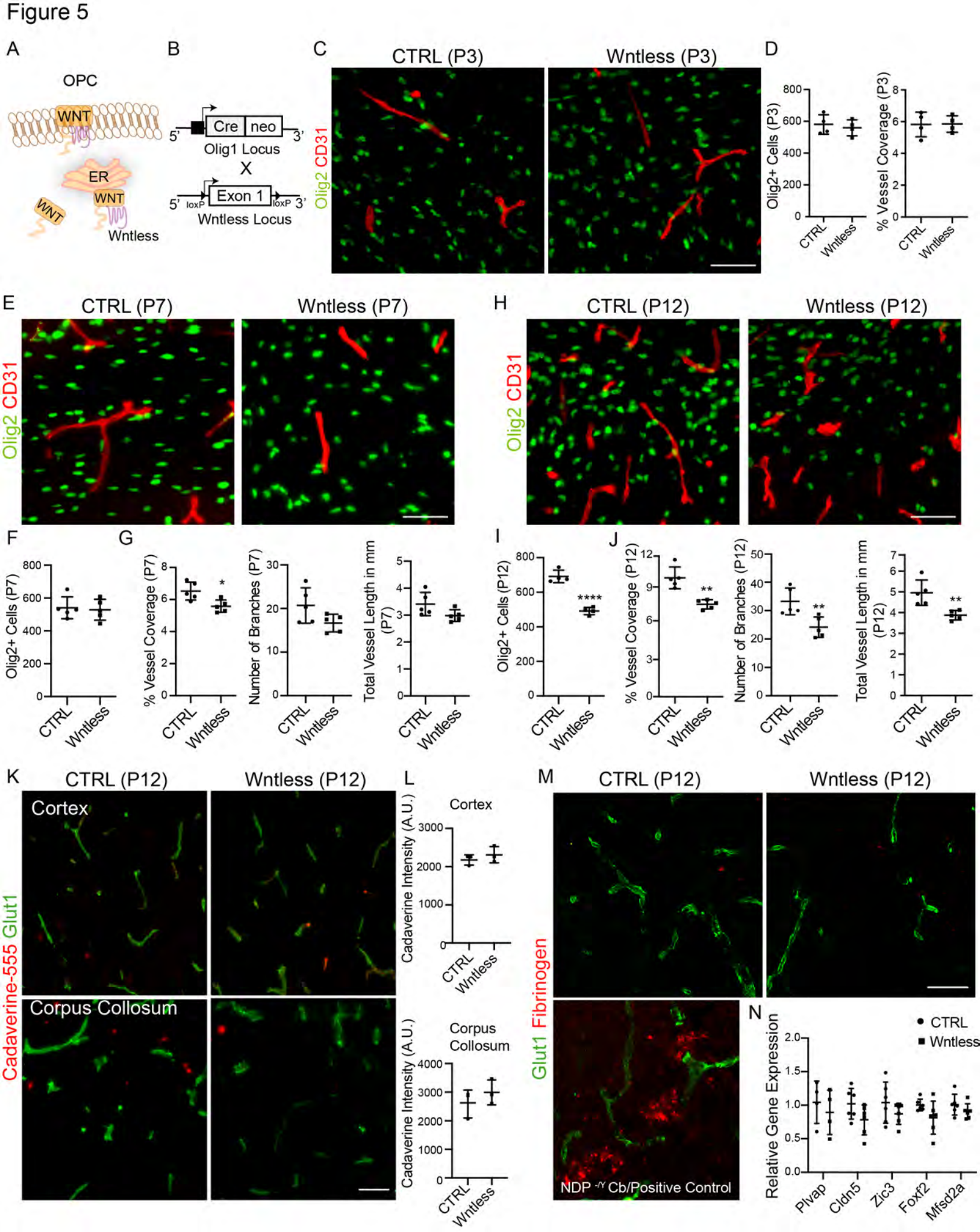
A
OPC
WNT
ER
WNT
WNT
Wntless
B
Cre
neo
5'
3'
Olig1 Locus
X
Exon 1
loxP
loxP
5'
3'
Wntless Locus
C
CTRL (P3)
Wntless (P3)
Olig2 CD31
D
Olig2+ Cells (P3)
% Vessel Coverage (P3)
CTRL
Wntless
E
CTRL (P7)
Wntless (P7)
Olig2 CD31
H
CTRL (P12)
Wntless (P12)
Olig2 CD31
F
Olig2+ Cells (P7)
G
% Vessel Coverage (P7)
Number of Branches (P7)
Total Vessel Length in mm (P7)
I
Olig2+ Cells (P12)
J
% Vessel Coverage (P12)
Number of Branches (P12)
Total Vessel Length in mm (P12)
K
CTRL (P12)
Wntless (P12)
Cortex
Corpus Collosum
Cadaverine-555 Glut1
L
Cortex
Corpus Collosum
Cadaverine Intensity (A.U.)
M
CTRL (P12)
Wntless (P12)
Glut1 Fibrinogen
NDP -/Y Cb/Positive Control
N
CTRL
Wntless
Relative Gene Expression
Plvap
Cldn5
Zic3
Foxf2
Mfsd2a

Figure 6

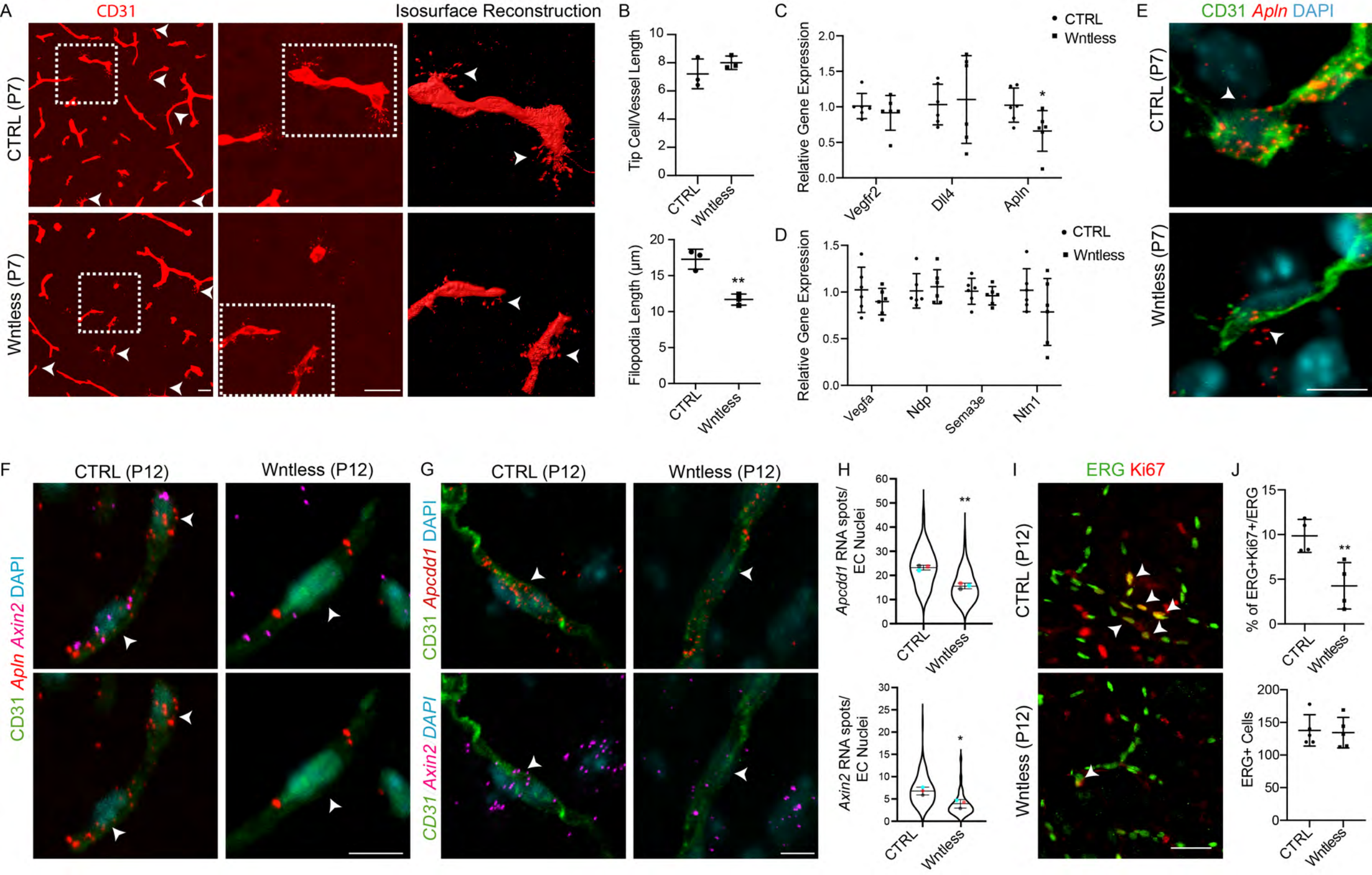
A
CD31
Isosurface Reconstruction
CTRL (P7)
Wntless (P7)
B
Tip Cell/Vessel Length
CTRL
Wntless
Filopodia Length (μm)
**
C
CTRL
Wntless
Relative Gene Expression
Vegfr2
Dll4
Apln
*
D
Vegfa
Ndp
Sema3e
Ntn1
E
CD31 Apln DAPI
F
CTRL (P12)
Wntless (P12)
CD31 Apln Axin2 DAPI
G
CD31 Apcdd1 DAPI
CD31 Axin2 DAPI
H
Apcdd1 RNA spots/ EC Nuclei
Axin2 RNA spots/ EC Nuclei
I
ERG Ki67
J
% of ERG+Ki67+/ERG
ERG+ Cells

Figure 7

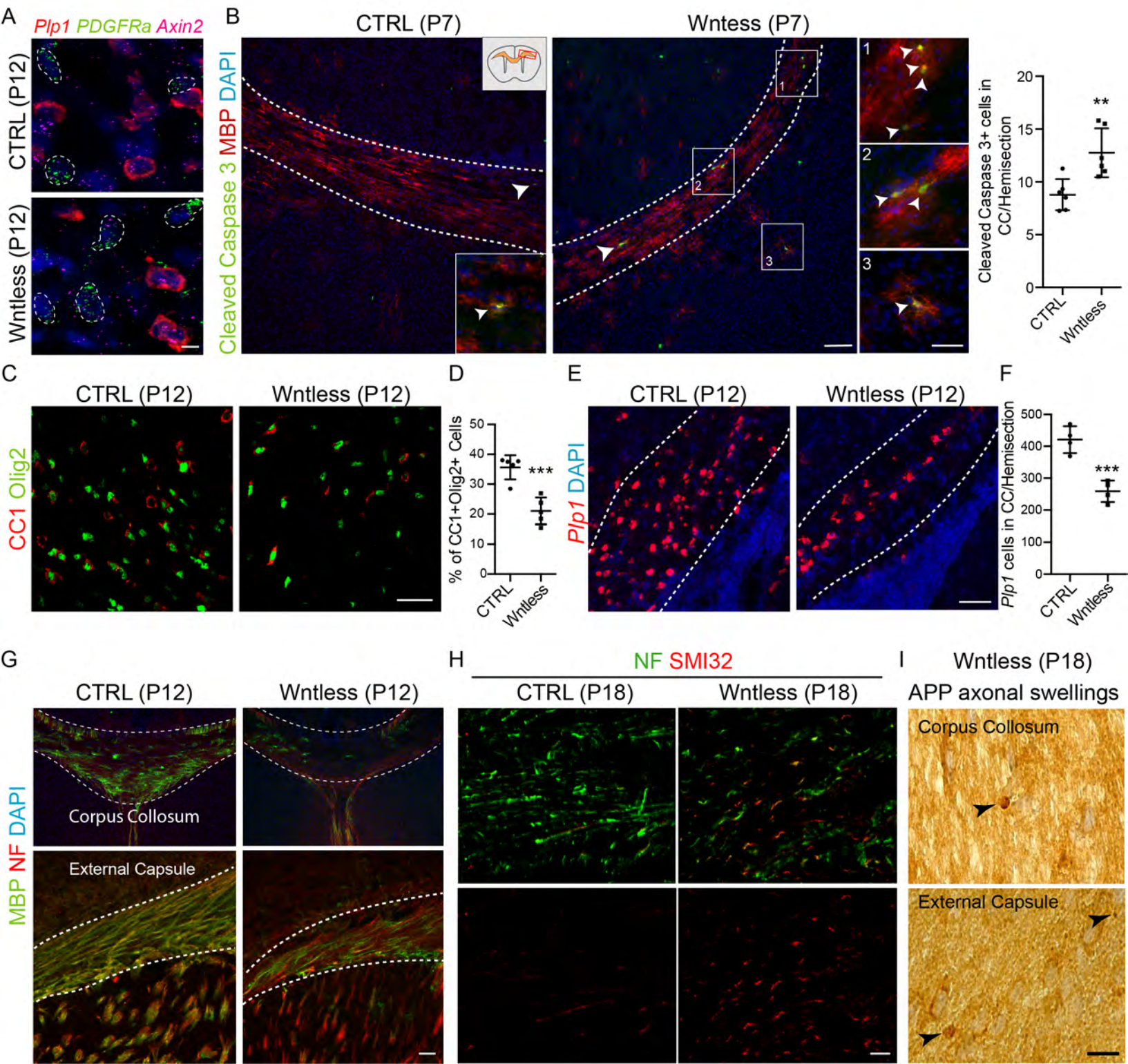
A
Plp1 PDGFRa Axin2
CTRL (P12)
Wntless (P12)
B
CTRL (P7)
Wntess (P7)
Cleaved Caspase 3 MBP DAPI
1
2
3
Cleaved Caspase 3+ cells in CC/Hemisection
20
15
10
5
0
**
CTRL
Wntless
C
CTRL (P12)
Wntless (P12)
CC1 Olig2
D
% of CC1+Olig2+ Cells
50
40
30
20
10
***
CTRL
Wntless
E
CTRL (P12)
Wntless (P12)
Plp1 DAPI
F
Plp1 cells in CC/Hemisection
500
400
300
200
100
***
CTRL
Wntless
G
CTRL (P12)
Wntless (P12)
Corpus Collosum
External Capsule
MBP NF DAPI
H
NF SMI32
CTRL (P18)
Wntless (P18)
I
Wntless (P18)
APP axonal swellings
Corpus Collosum
External Capsule

Figure 8

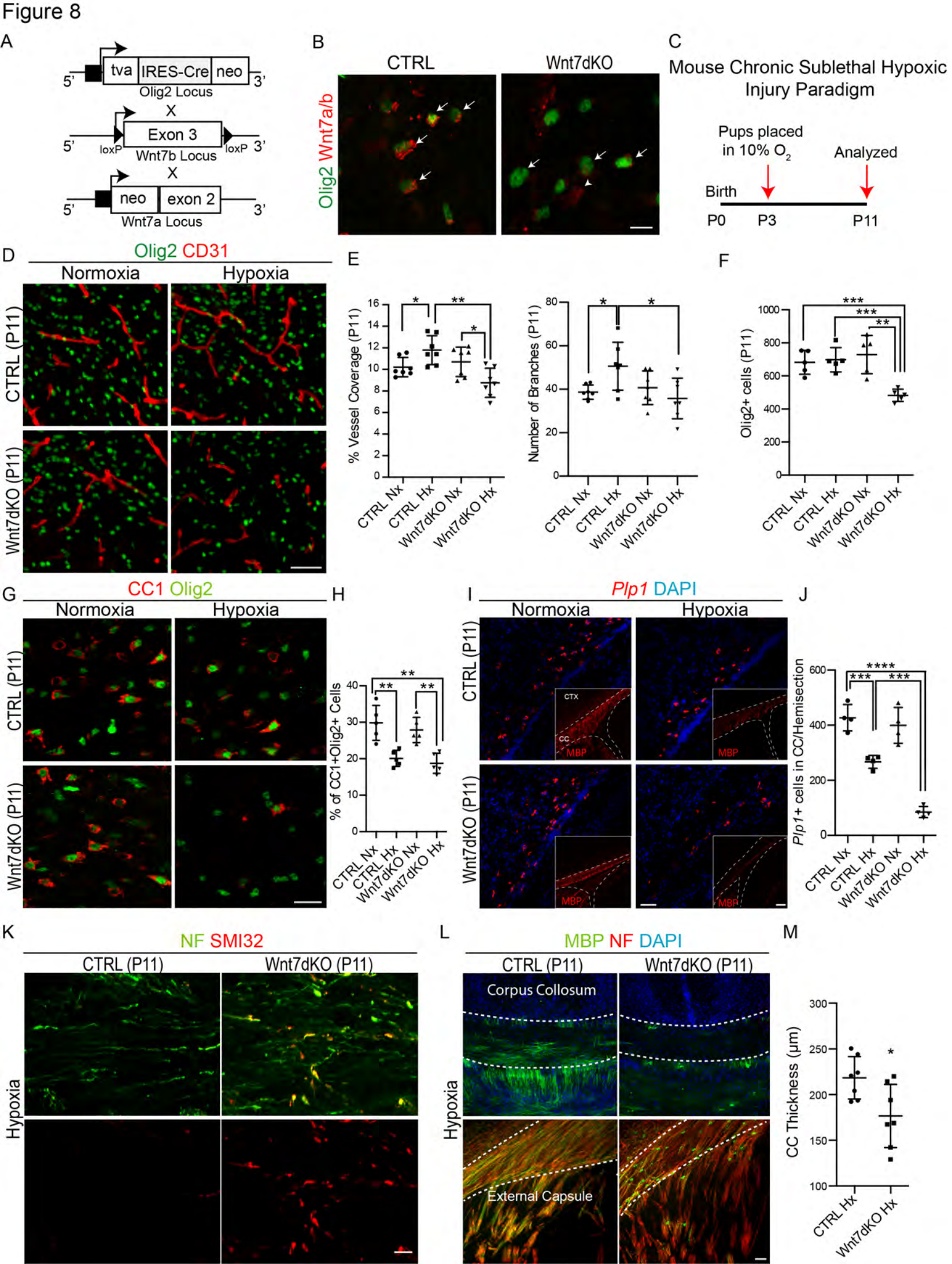
A
tva
IRES-Cre
neo
5'
3'
Olig2 Locus
X
Exon 3
loxP
loxP
Wnt7b Locus
neo
exon 2
Wnt7a Locus
B
CTRL
Wnt7dKO
Olig2 Wnt7a/b
C
Mouse Chronic Sublethal Hypoxic Injury Paradigm
Pups placed in 10% O2
Analyzed
Birth
P0
P3
P11
D
Olig2 CD31
Normoxia
Hypoxia
CTRL (P11)
Wnt7dKO (P11)
E
% Vessel Coverage (P11)
Number of Branches (P11)
CTRL Nx
CTRL Hx
Wnt7dKO Nx
Wnt7dKO Hx
F
Olig2+ cells (P11)
G
CC1 Olig2
H
% of CC1+Olig2+ Cells
I
Plp1 DAPI
CTX
CC
MBP
J
Plp1+ cells in CC/Hemisection
K
NF SMI32
L
MBP NF DAPI
Corpus Collosum
External Capsule
M
CC Thickness (µm)

Star Methods

Animals

All animal procedures were performed according to the University of California at San Francisco guidelines under Institutional Animal Care and Use Program (IACUC)-approved protocols. Age of the mice/ferrets used for the study are identified in the main text and figure legends. Both male and female animals were used in this study.

Olig2-cre mouse line was previously described (Schuller et al., 2008) . Briefly, the line was generated by inserting an avian-specific retroviral receptor, and an IRES-cre recombinase cassette into the endogenous Olig2 locus by homologous recombination.

Sox10-DTA mice have been generated by Dr. William Richardson's lab and are previously described (Kessaris et al., 2006).

$BRAF^{CA}$ is a knock-in allele of human BRaf which expresses normal BRaf prior to Cre recombinase exposure and encodes mutationally activated $BRAF^{V600E}$ after Cre recombination (Dankort et al., 2009).

Olig1-Cre mouse line was generated by inserting a cre-neo cassette into the Olig1 locus via homologous recombination and was previously described (Lu et al., 2002).

Wntless floxed mice were purchased from Jackson laboratory (Stock No:012888) and are previously described (Carpenter et al., 2010).

Wnt7dKO mice were generated by intercrossing *Olig2-Cre* mouse line to *Wnt7a+/-* and *Wnt7b (fl/fl)* lines (Stenman et al., 2008). Note that Wnt7a-/- mice are infertile so they were bred as heterozygotes.

Mouse Chronic Sublethal Hypoxia

Chronic hypoxic rearing was performed as previously described (Yuen et al., 2014). Briefly, litters from Control or *Wnt7dKO* animals were culled to a size of 4 pups and co-fostered with CD1 strain dams then reared at 10% O_2 in a hypoxic chamber starting on postnatal day 3 (P3) (Biospherix, Inc., Laconia, NY). Tissue from P11 pups were then harvested for analysis.

Ferret Chronic Sublethal Hypoxia

Pregnant jills were obtained from Marshall Farms (North Rose, NY) at E26 gestation. The kits from these ferrets along with the jill were placed in a 10% oxygen chamber on postnatal day 10 (P10) until P20 endpoint. Kits were euthanized within 1 hour after removal from their housing by deeply anesthetizing with isoflurane in an anesthesia chamber. After loss of righting reflex, the animals were transcardially perfused with PBS followed by 4% PFA. Following perfusion, brains were removed from the skull using forceps or a bone rongeur.

Human Developmental Tissue.
This study involves use of de-identified human post-mortem fixed-frozen brain tissue samples obtained from University of California, San Francisco's Pediatric Neuropathology Research Laboratory. Tissue was fixed with 4% paraformaldehyde, followed by sequential immersion in 10%, 20% and 30% sucrose for cryopreservation. Frozen tissues are sectioned at 14 µm for immunohistochemistry and smFISH applications. All the HIE cases in this study showed evidence of diffuse white matter injury, with astrogliosis and macrophage infiltration (Supplementary Figure 3). It must be noted that although some control brain specimens were obtained from diaphragmatic hernia cases, which may result in hypoxemia, these specimens were examined and classified as "control" by an experienced neuropathologist and did not exhibit any evidence of astrogliosis or macrophage infiltration.

Tissue Processing and Immunohistochemistry
Mice were deeply anesthetized and transcardially perfused with cold PBS followed by cold 4% PFA. Brains were isolated and post-fixed overnight in 4% PFA and cryo-protected in 30% sucrose for 24 hours and then frozen at -80°C until sectioned. Frozen brains were sectioned at 30µm thickness. Tissue sections were blocked for 1 hour using blocking solution (5% horse serum/0.3% Triton X-100 in PBS) and incubated with primary antibodies (resource table) overnight at 4°C in fresh blocking solution. Sections were washed thrice in PBS containing 0.4% Triton X-100 followed by incubation with the appropriate secondary antibodies purchased from Invitrogen. Three to five additional washes were performed, and sections were mounted using DAPI-Fluoromount G (SouthernBiotech). Antigen retrieval was performed by pre-treating the sections for 10 minutes at 95°C in 10mM Sodium Citrate (pH 6.0) in a microwave oven (BioWave). Histological preparations were analyzed using Leica Sp5 upright AOBS confocal microscope. Images were acquired with either 20x, 40x or 63x objectives.

Olig2 Immunogold Labeling and Electron Microscopy Processing
The specimen was obtained by a surgical resection of the right temporal lobe from a 2-year old female with type IIB focal cortical dysplasia patient. The tissue was fixed in 4% PFA in 0.1M PBS for 7 days. After 100 µm sections were obtained using a using a Leica VT1000S vibratome (Leica Biosystems, Wetzlar, Germany). For pre-embedding immunogold, the tissue was cryoprotected in a solution containing 25% saccharose in 0.1M phosphate buffer (PB) for 30 min followed by repeated freeze-thaw cycles for permeabilization. The permeabilization step was performed by immersing the samples repeatedly in -60ºC 2-methylbutane and transferring them to room temperature saccharose solution. After, the samples were incubated in a blocking solution consisting of 0.3% BSAc (Aurion, Wageningen, the Netherlands), 0.05% sodium azide in 0.1 M PB for 1 h. Subsequently, the samples were incubated in primary antibody (1:150 rabbit anti-Olig2, Millipore) in blocking solution for 72 h at 4ºC. The sections were then rinsed in 0.1 M PB and incubated in secondary antibody blocking solution consisting of 0.5% BSAc (Aurion), 0.025% CWFS gelatin (Aurion), 0.05% sodium azide in 0.1 M PB for 1 h, followed by incubation in secondary antibody (1:50 goat-anti-rabbit IgG gold ultrasmall; Aurion) diluted in the same solution overnight at 4ºC. To enhance gold labeling, we performed silver enhancement (R-GENT SE-LM, Aurion) for 15–25 min in the dark,

followed by gentle washing in 2% sodium acetate and incubation in gold toning solution (0.05% gold chloride in water) for 10 min. The sections were then washed twice with 0.3% sodium thiosulfate in water. Finally, we post fixed with 2% glutaraldehyde (Electron Microscopy Sciences) in 0.1M PB for 30 min.

For transmission electron microscopy analysis, specimen was post fixed with 1% osmium tetroxide (Electron Microscopy Sciences), 7% glucose in 0.1M PB for 30 min at room temperature, washed in deionized water, and partially dehydrated in 70% ethanol. Afterwards, the samples were contrasted in 2% uranyl acetate (Electron Microscopy Sciences) in 70% ethanol for 2 hours at 4ºC. The samples were further dehydrated and embedded in Durcupan ACM epoxy resin (Sigma-Aldrich) at room temperature overnight, and then at 60ºC for 72 h. Once the resin was polymerized, immunolabeled sections were selected and cut into semithin (1.5 μm) and ultrathin (60–80 nm) sections using a UC6 ultramicrotome (Leica Biosystems). These sections were placed on Formvar-coated single-slot copper grids (Electron Microscopy Sciences) stained with lead citrate and examined at 80 kV on a FEI Tecnai G2 Spirit (FEI Company, Hillsboro, OR) transmission electron microscope equipped with a Morada CCD digital camera (Olympus, Tokyo, Japan).

Single molecule fluorescent *in situ* hybridization

Three-color smFISH was performed on fixed frozen sections from human neonatal brain specimen or control and mutant mice using Advanced Cell Diagnostics RNAscope® Fluorescent Multiplex Reagent Kit and probes. Cryosections (14µm thick) were mounted on glass slides and washed in RNase free PBS for 5 mins. Slides were then baked at 60°C for 30 mins and were further fixed in 4% neutral buffered paraformaldehyde for 15 min at 4°C. Next, sections were dehydrated in 50%, 70% and 100% ethanol for 5 mins at room temperature and air dried. Target retrieval was then performed with RNAscope reagents for 5 mins at 95 °C for human and 2 minutes for mouse tissue respectively and sections were further washed with distilled water followed by washes in 100% ethanol 2-3 times. Sections were next treated with Protease IV reagent for 30 mins at 40°C (for human tissue) or Protease III reagent for 15 minutes at 40°C (for mouse tissue). Sections were then washed and maintained in RNase free water until hybridization step. Probes listed in the resource table were diluted at 1:50 ratio in channel 1 probe and preheated to 40°C for 5 mins and sections were incubated with this probe mix for 2hr at 40°C. After probe hybridization, sections were washed twice for 2 mins each before proceeding to the fluorescent detection step according to manufactures protocol. Briefly sections were incubated in AMP 1-FL for 30 min at 40°C, washed two times, incubated in RNAscope AMP 2-FL for 15 min at 40°C, washed two times, incubated in RNAscope AMP 3-FL for 30 min at 40°C, washed two times and incubated in AMP 4-FL-Alt B solution for 15 mins at 40°C, washed two times before IHC labelling (see above). If IHC was not required, sections were counterstained with RNAscope DAPI for 30 seconds after final detection step. All wash steps were performed with RNAscope 1x wash buffer. Quantification of RNA spots was performed on images acquired at 63x on Lecia SP5 upright AOBS confocal microscope. RNAspots were quantified from atleast 100 cells from images obtained from different human cases/condition or animals/genotype and represented as

SuperPlots (Lord et al., 2020).

Cadaverine Permeability Assay
Lysine-fixable, cadaverine conjugated to Alexa Fluor-555 (ThermoFischer Scientific) was injected intraperitoneally at 25mg/kg and the mouse pups were sacrificed after 2 hours and the brains were isolated as described above. Cadaverine leakage was quantified by mean pixel intensity, measured from different microscopic fields from atleast 3 sections from three animals each per genotype.

Quantitative PCR Analysis
White matter tissue isolates were obtained from P8-P10 control or *Wntless* cKO mice and lysed with Qiazol (Qiagen) and RNA was isolated with the RNeasy Kit (Qiagen) following manufacture's protocol. Total RNA was reverse transcribed to cDNA using SuperScript IV First-Strand Synthesis System (Invitrogen) for quantitative-PCR experiments (qPCR). Using the transcript specific primers (Table S2), cDNA was amplified, and qPCR was performed using the Roche 480 LightCycler and SYBR Green-based Master Mix. Gene expression levels were calculated using the ΔΔCt method and normalized using *GAPDH* as a reference.

Microscopy and Cell Counting
Optical sections of confocal epifluorescence images were sequentially acquired using LAS AF software (Leica). Images were merged using ImageJ software and merged images were processed on Adobe Illustrator software. In some cases, background modifications, which were applied evenly across the entire image and between control and experimental groups were performed for presentation purposes on LAS AF software or ImageJ. At least n=4-7 different animals for each experimental condition were collected and analyzed as indicated in the respective figure legends. Matched sections between -2.0 and +1.10 bregma were used for analysis and the regions indicated in Figure 1E were analyzed. Typically, 3-6 fields from 6-8 non-adjacent sections were analyzed per animal and counts are presented as the number cells per 1 mm^2 or percentage of cells within the indicated cell population. All counts were performed using ImageJ software.

Vascular Density, Branching and Length Quantifications
Images were obtained as above from regions of interest (Corpus collosum, cingulum and external capsule from various rostro-caudal levels) and vascular coverage was analyzed on ImageJ. Vessel images were segmented on Image J and the percentage of vessel coverage was determined by quantifying the percent of the vessel segmented area over the total imaged area. Vessel branching was manually counted from the images obtained from atleast 40-50 fields from different white matter and cortical regions from n=4-7 animals as mentioned in figure legends. Total vascular length was quantified as the sum of lengths of all vessels in a field using the angiotool (Zudaire et al., 2011) image J plugin.

Statistics

Data shown are represented as mean ± S.D. and the number of experiments/animals per genotype is indicated in each case in figure legends. Statistical analysis was performed using the two tailed unpaired Student's t-test. A “p” value < 0.05 was considered significant. In all cases, * indicates a p value <0.05, **<0.01, and ***p<0.001, **** p<0.0001. All the data analysis and plotting were performed on GraphPad Prism version 6.0.

Reagent and Resource Table

Antibody/Reagent	Catalogue Number	Species
CD31/PECAM	ABCAM: ab28364	Rabbit
CD31/PECAM	ABCAM: ab9498	Mouse
CD31/PECAM	BD Biosciences 550274	Rat
Collagen 4a	Millipore: AB769	Goat
Olig2	R&D Systems-AF2418	Goat
Lef1 (C12A5)	Cell signaling-2230	Rabbit
APP A4 Antibody	Millipore: MAB348	Mouse
SMI32 (Nonphosphorylated; NF-H)	Biolegend- 801702	Mouse
Neurofilament H (SMI312)	Biolegend- 837904	Mouse
Neurofilament H	Encor Biotech CP-CA-NFH)	Chicken
ERG	Cell signaling-97249	Rabbit
Ki67	BD Biosciences 550609	Mouse
PDGFRa	Cell signaling, mAb 3174	Rabbit
PDGFRa	Gift from Bill Stallcup	Human
Olig2	Gift from C. Stiles, Harvard	Mouse
Claudin 5 (4C3C2)	Invitrogen: 35-2500	Mouse
Iba1	Wako 019-19741	Rabbit
GFP	Aves Labs-GFP-1010	Chicken
Glut1	Millipore, 07-1401	Rabbit
PDGFRb	Invitrogen 14-1402-81	Rat
Plvap (MECA-32)	BD Biosciences 550563	Rat
Aquaporin-4	Millipore AB3594	Rabbit
BCAS1	Santa Cruz sc-393740	Mouse
Nogo-A	R&D Systems MAB3098	Mouse
TCF4 (Clone 6H5-3)	Millipore-05-511	Mouse
MBP	Millipore MAB386	Rat

Cleaved Caspase-3	Cell Signaling #9661	Rabbit
Wnt7	Santa Cruz sc-26361	Goat
APC (CC-1)	Millipore OP80	Mouse
GFAP (2.2B10)	Invitrogen 13-0300	Rat
CD68	BD Biosciences 556059	Mouse
RNAScope PDGFRa-Hs Probe	ACD Bio 604481-C2	Human
RNAScope Olig2-Hs Probe	ACD Bio 424191-C3	Human
RNAScope Apcdd1-Hs Probe	ACD Bio 535851-C2	Human
RNAScope Axin2-Hs Probe	ACD Bio 400241-C3	Human
RNAScope Wnt7a-Hs Probe	ACD Bio 408231-C1	Mouse
RNAScope PDGFRa-Mm Probe	ACD Bio 480661-C2	Mouse
RNAScope Apcdd1-Mm Probe	ACD Bio 425701-C1	Mouse
RNAScope Axin2-Mm Probe	ACD Bio 400331-C3	Mouse
RNAScope Multiplex Fluorescent Kit	ACD Bio 320850	

Supplementary Table 1: Human postmortem cases analyzed in this study.

Identification	Neuropathology	Gestational age	Postnatal age	Sex	Clinical Diagnosis
UCSF 2010-008	Control	36 Weeks	0 Days	F	Diaphrgmatic Hernia
UCSF 2010-013	Control	37 Weeks	2 Days	F	Pneumothraces
UCSF 2010-005	Control	40 Weeks	0 Days	M	Diaphragmatic Hernia
UCSF 2010-012	Control	40 Weeks	2 Days	M	Diaphragmatic Hernia
UCSF 2017-032	Control	37 Weeks	2 Days	M	Hydronephrosis
UCSF 2012-003	Control	36 Weeks	10 Days	M	VATER malformation
UCSF 2010-019	HIE	35 Weeks	6 Days	M	Unknown/IVH
UCSF 2011-005	HIE	40 Weeks	3 Days	M	Placental abruption
UCSF 2013-008	HIE	39 Weeks	1 day	M	Fetal Bradycardia
UCSF 2010-016	HIE	37 Weeks	5 Days	F	Birth Asphyxia
UCSF 2017-027	HIE	40 Weeks	9 Days	F	Pulmonary hypertension
UCSF 2012-001	HIE	38 Weeks	3 Days	F	Birth Asphyxia
UCSF 2016-004	Control	17 Weeks	0 Days		Tetralogy of fallot

Supplementary Table 2: Primer sequences used in this study.

Plvap	F	GTTGACTACGCGACGTGAGATG
	R	AGCTGTTCCTGGCACTGCTTCT
Claudin 5	F	TGACTGCCTTCCTGGACCACAA
	R	CATACACCTTGCACTGCATGTGC
Zic3	F	CACACTGGCGAGAAACCCTTCC
	R	GTTGGCAAACCGTCTGTCACAG
Foxf2	F	CCAGCATGTCTTCCTACTCGTTG
	R	CTTTCCTGTCGCACACTGGAGT
Mfsd2a	F	GGTCTCAGAAGTTGCCAATCGC
	R	GAAGGCACAGAGGACGTAGATG
Vegfr2	F	CGAGACCATTGAAGTGACTTGCC
	R	TTCCTCACCCTGCGGATAGTCA
Dll4	F	GGGTCCAGTTATGCCTGCGAAT
	R	TTCGGCTTGGACCTCTGTTCAG
Apln	F	AGGCATAGCGTCCTCACCTCTT
	R	GGTGCAGAAACGACAAAGACGG
Vegfa	F	CTGCTGTAACGATGAAGCCCTG
	R	GCTGTAGGAAGCTCATCTCTCC
Ndp	F	CTGATGGACTCTCAACGCTGCA
	R	CTCAGAGCGTGATGCCTGGCT
Sema3e	F	CACTGTGCCTTCATCAGAGTCG
	R	CCAACTAGCGTGGACACAAAGG
Ntn1	F	GTCTGGTGTGTGACTGTAGGCA
	R	CCGAGCATGGAGGTTGCAGTTG

Supplementary Figure Legends

Supplementary Figure 1: Characterization of Glial-Endothelial Tip Cell Interactions. (Related to Figure 1)

(A) Representative images from P1 mouse brain labelled with Iba1 and CD31 show that microglial cells (Iba1+ cells) don't frequently contact endothelial tip cells in developing white matter. Scale bar: 25μm.
(B) Representative images from 17GW human brain labelled with Iba1 and CD31 show that microglial cells (Iba1+ cells) don't frequently contact endothelial tip cells in developing deep cortical regions adjacent to the ventricle. Scale bar: 25μm.
(C-D) Representative images from 17GW human brain coronal sections labelled with GFAP (C), PDGFRa (D) and CD31. Isosurface reconstruction of highlighted region shows that PDGFRa+ OPCs but not GFAP+ astroglial cell processes make complex contacts with endothelial tip cells at the sites where neighboring vessels fuse. Scale bar: 25μm.
(E) Representative images from P11 *Sox10-GFP* transgenic mouse labelled with CD31 show that OPC-endothelial tip cell contacts persist into late postnatal stages in white matter. Scale bar: 25μm.

Supplementary Figure 2: Characterization of *Olig2-Cre/Sox10-DTA* model. (Related to Figure 2)

(A) Lineage tracing analysis reveals that ~75% of oligodendroglial cells in the white matter are targeted by *Olig2-Cre* line. Scale bar: 50μm.
(B) Representative images from P1 Control and *Sox10-DTA* white matter shows oligodendroglial targeting by *Sox10-DTA* strategy. Scale bar: 50 μm.
(C) Oligodendroglial cells that escape recombination by either *Olig2-Cre* or *Sox10-DTA* strategy proliferate in an effort to repopulate the brain. Scale bar: 50 μm.
(D) Coronal brain sections from control and *Sox10-DTA* mice at P11 shows repopulation of oligodendroglial cells. *Sox10-DTA* animals remain hypomyelinated at P11. Scale bar: 100 μm.
(E) Oligodendroglial ablation in *Sox10-DTA* did not cause BBB disruptions as revealed by lack of Claudin5 negative PLVAP positive endothelial cells. Insets in bottom panel represent positive control for PLVAP labelling, showing PLVAP+ vessels in choroid plexus from the same section. Scale bar: 50μm.
(F) Astrocyte endfeet coverage abnormalities were not observed in *Sox10-DTA* mice. Scale bar: 50μm.
(G) No microglial (Iba1+) or astroglial reactivity (GFAP+) were not observed in *Sox10-DTA* white matter. Scale bar, 50μm.
(H) Representative images from corpus collosum region of Cadaverine-555 injected control and *Sox10-DTA* mice labelled with Glut1. Note no leakage of cadaverine-555 in *Sox10-DTA* animals, indicating no damage to BBB. Scale bar: 50μm.

Supplementary Figure 3: Characterization of *BRAF^{CA}* Forebrain White Matter. (Related to Figure 3)

(A) *BRAF^{CA}* mice survive until second postanal week (P14) and do not form neoplasms. Scale bar: 100 μm.

(B) Hypervascularization of *BRAF*^{CA} forebrain white matter was evident at P14. Scale bar: 50μm.
(C) Mild decrease in myelin levels (MBP) were observed in *BRAF*^{CA} forebrain white matter at P14, when they begin to display motor abnormalities. Scale bar: 100μm.
(D) Representative images of white matter region from CTRL and BRAF^{CA} brain sections labelled with Claudin 5 and Glucose transporter 1 (Glut1). Note the absence of Claudin 5 and Glut1 negative vessels, indicating no blood brain barrier (BBB) damage. Quantification of Claudin 5+ vessel coverage in white matter showing no tight junction disruptions. Scale bars: 50μm. Data shown as mean ± S.D. and analyzed by a two-tailed unpaired Student's t test. n=3 animals/genotype for data shown in (B) and n=5 for (D); *p<0.05.

Supplementary Figure 4: OPC Density Does Not Alter Forebrain Cortical Vascular Coverage. (Related to Figures 2 and 3)
(A) Representative images from P11 - Control (CTRL) and *Sox10-DTA* mouse coronal brain sections labelled with CD31 showing no alterations in cortical vascular coverage. Scale bar: 100μm Ctx: Cortex, CC: Corpus Collosum.
(B) Boxed regions from (A), showing decrease in Olig2+ cell numbers but not vascular coverage. Scale bar: 50μm.
(C) Quantification of Olig2+ cell numbers and vascular coverage from forebrain cortical regions of P1 and P11 CTRL and *Sox10-DTA* mice.
(D) Representative images from P9 - Control (CTRL) and *BRAF*^{CA} mouse coronal brain sections labelled with CD31 showing no alterations in cortical vascular coverage. Scale bar: 100μm
(E) Boxed regions from (D), showing increase in Olig2+ cell numbers but not vascular coverage. Scale bar: 50μm.
(F) Quantification of Olig2+ cell numbers and vascular density from forebrain cortical regions of P0 and P9 CTRL and *BRAF*^{CA} mice. Data shown as mean ± S.D. and analyzed by two-tailed unpaired Student's t test. n=4-5 animals/genotype for data shown in C and F. **p<0.01, ***p<0.001, **** p<0.0001. Ctx: Cortex, CC: Corpus Collosum.

Supplementary Figure 5: Characterization of Hypoxic Lesions in Human and Ferret Brain. (Related to Figure 4)
(A) Increase in astrogliosis and macrophage infiltration in HIE lesions revealed by GFAP and CD68 immunostaining. Scale bar: 50μm.
(B) Claudin 5+ junctional coverage on the vessels was not affected in the HIE white matter lesions. Scale bar: 50μm.
(C) Higher numbers of Lef1+ endothelia in vessels that are in closer apposition to Olig2+ cells in 23 Gestational Weeks (GW) developing human brain. Scale bar: 50μm.
(D) Multiplex smFISH of *Wnt7a* and *Olig2* in HIE white matter lesions. Scale bar: 10μm.
(E) RNAScope positive (*PPIB;* top panel) and negative (*dapB; bottom panel*) controls from human brain tissue. Scale bar: 25μm.
(F) Endothelial cells in the white matter lesions of HIE cases showed higher Lef1+ expression. Scale bar: 50μm.

(G) Increase in Lef1+ endothelial cells in white matter tracts of ferrets reared in hypoxia. Scale bar: 50μm.
(H) Quantification of ERG+ and Lef1+ endothelial cells in normoxic and hypoxic ferret brain white matter tracts. Data shown as mean ± S.D. and analyzed by a two-tailed unpaired Student's t test. n=3 animals per condition for data represented in (H), *p<0.05. n.s. not significant.

Supplementary Figure 6: Additional Characterization of P12 *Wntless* cKO Animals. (Related to Figure 5)
(A) Immunostaining for Claudin 5, Glut1 (top panels) and PLVAP (bottom panels) did not reveal any blood brain barrier (BBB) disruptions in *Wntless* cKO brain. Scale bar: 50μm.
(B) Mild astroglial reactivity was noticed in the *Wntless* cKO forebrain white matter region but microglial inflammatory response was not observed. Scale bar: 50μm.
(C) Proliferation of oligodendroglial cells is not affected in *Wntless* cKO white matter at P12. Scale bar: 25μm.
(D) Oligodendroglial Wnt downstream signaling is not affected in *Wntless* cKO white matter as revealed by TCF4 expression in Olig2+ cells. Scale bar: 25μm. Data are shown as mean ± S.D. and were analyzed by two-tailed unpaired Student's t test, n=5 animals/genotype for data represented in (C).

Supplementary Figure 7: Additional Characterization and Controls Showing Oligodendroglial Wnt7a/b are Required for Activation of Endothelial Wnt Signaling and Vessel Growth. (Related to Figure 8)
(A) Hypoxia induced vessel angiogenesis in white matter is associated with endothelial cell proliferation as revealed by increase in ERG+Ki67+ cells. Note, *Wnt7dKO* animals reared in hypoxia do not exhibit a similar proliferatory response observed in controls. Scale bar: 25μm.
(B) Quantification of endothelial cell proliferation (ERG/Ki67) in control and *Wnt7dKO* animals reared in normoxic and hypoxic conditions.
(C-D) Multiplex smFISH to label *Apcdd1* (C) and *Axin2* (D) reveals hypoxia induced increase in downstream Wnt signaling in endothelial cells of white matter at P11. Note this response was reduced in *Wnt7dKO* animals reared in hypoxia. Scale bar: 5 μm.
(E) Immunostaining for PLVAP and Claudin 5 did not reveal any BBB disruptions in *Wnt7dKO* animals. Inset in bottom right panel shows PLVAP expression in choroid plexus vessels from the same section confirming successful PLVAP labelling. Scale bar: 50μm.
(F) Representative images from corpus collosum region of Cadaverine-555 injected control and *Wnt7dKO* animals labelled with Glut1. Note no leakage of cadaverine-555 in *Wnt7dKO* animals, indicating no damage to BBB. Scale bar: 50μm.
(G) No alterations were observed in inflammatory responses (Iba1) or astroglial reactivity (GFAP) in hypoxic *Wnt7dKO* animals. Scale bar: 50μm.
(H) Genetic ablation of *Wnt7a* or *Wnt7b* alone do not contribute to hinderance in post hypoxic injury white matter angiogenesis as revealed by CD31 immunostaining. Scale bar: 50μm

(I) Quantification of vessel coverage in WT, *Wnt7a-/-* and *Olig2-Cre/Wnt7b (fl/fl)* animals reared in hypoxia. For all quantifications data are shown as mean ± S.D. and are analyzed by a two-tailed unpaired Student's t test. n=3 animals/genotype per condition for data represented in (B) and (I) Significance between two groups are shown as *p<0.05, ***p<0.001.

Supplementary Figure 8: Additional Characterization of White Matter and Cortical Oligodendroglial Development in *Wnt7dKO* Mutants. (Related to Figure 8)
(A) Representative images from P7 white matter region of control and *Wnt7dKO* animals reared in hypoxia showing Olig2+ oligodendroglial cells and Col4a+ blood vessels. Note a decrease in blood vessel density compared to control. Scale bar: 50μm.
(B) Quantification of P7 white matter Olig2+ cell numbers and vessel coverage.
(C) Hypoxic *Wnt7dKO* animals show increase in apoptosis marker, cleaved caspase 3 in white matter regions, cingulum and external capsule at P7 compared to control animals reared in hypoxia. Scale bar: 50μm.
(D) Cortical PDGFRa+Olig2+ oligodendroglial precursor cell numbers were not affected by hypoxia in *Wnt7dKO* animals. Scale bar: 50μm.
(E) Quantification of Olig2+ oligodendroglial and PDGFRa+Olig2+ oligodendroglial precursor cell numbers in cortex. Data shown as mean ± S.D. and are analyzed by a two-tailed unpaired Student's t test and n=3 animals/genotype per condition for data represented in (B) and n=4 for (E).

Description of Supplementary Video S1
Video showing hind limb clasping and tremors in *Wntless* cKO mouse (on right) compared to a littermate control (on left) that appears normal.

Supplementary References

1. Carpenter, A.C., Rao, S., Wells, J.M., Campbell, K., and Lang, R.A. (2010). Generation of mice with a conditional null allele for Wntless. Genesis *48*, 554-558.
2. Dankort, D., Curley, D.P., Cartlidge, R.A., Nelson, B., Karnezis, A.N., Damsky, W.E., Jr., You, M.J., DePinho, R.A., McMahon, M., and Bosenberg, M. (2009). Braf(V600E) cooperates with Pten loss to induce metastatic melanoma. Nat Genet *41*, 544-552.
3. Kessaris, N., Fogarty, M., Iannarelli, P., Grist, M., Wegner, M., and Richardson, W.D. (2006). Competing waves of oligodendrocytes in the forebrain and postnatal elimination of an embryonic lineage. Nat Neurosci *9*, 173-179.
4. Lord, S.J., Velle, K.B., Mullins, R.D., and Fritz-Laylin, L.K. (2020). SuperPlots: Communicating reproducibility and variability in cell biology. J Cell Biol *219*.
5. Lu, Q.R., Sun, T., Zhu, Z., Ma, N., Garcia, M., Stiles, C.D., and Rowitch, D.H. (2002). Common developmental requirement for Olig function indicates a motor neuron/oligodendrocyte connection. Cell *109*, 75-86.
6. Schuller, U., Heine, V.M., Mao, J., Kho, A.T., Dillon, A.K., Han, Y.G., Huillard, E., Sun, T., Ligon, A.H., Qian, Y.*, et al.* (2008). Acquisition of granule neuron

precursor identity is a critical determinant of progenitor cell competence to form Shh-induced medulloblastoma. Cancer Cell *14*, 123-134.
7. Stenman, J.M., Rajagopal, J., Carroll, T.J., Ishibashi, M., McMahon, J., and McMahon, A.P. (2008). Canonical Wnt signaling regulates organ-specific assembly and differentiation of CNS vasculature. Science *322*, 1247-1250.
8. Yuen, T.J., Silbereis, J.C., Griveau, A., Chang, S.M., Daneman, R., Fancy, S.P.J., Zahed, H., Maltepe, E., and Rowitch, D.H. (2014). Oligodendrocyte-encoded HIF function couples postnatal myelination and white matter angiogenesis. Cell *158*, 383-396.
9. Zudaire, E., Gambardella, L., Kurcz, C., and Vermeren, S. (2011). A computational tool for quantitative analysis of vascular networks. PLoS One *6*, e27385.

Supplementary Figure 1

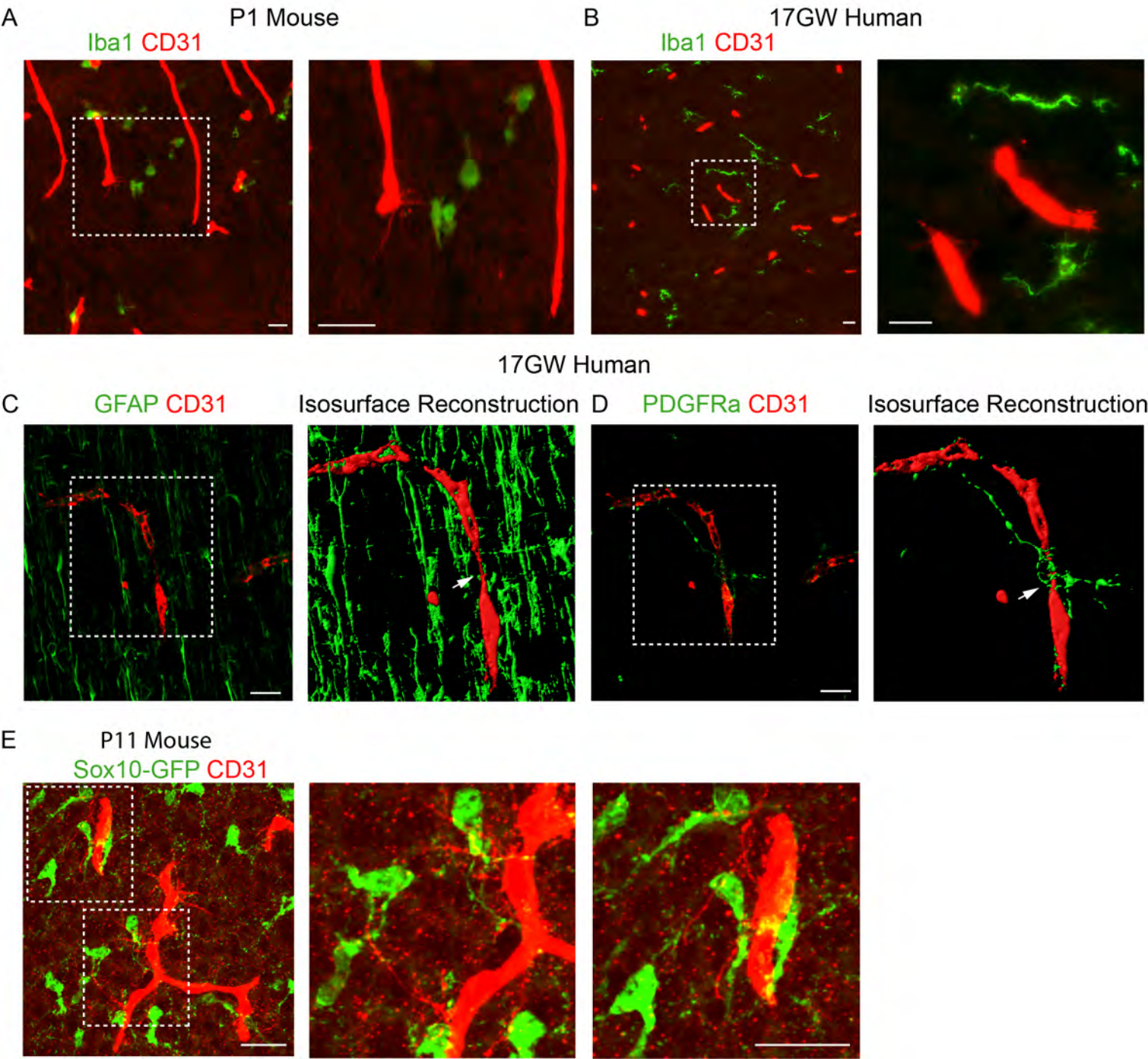

Supplementary Figure 2

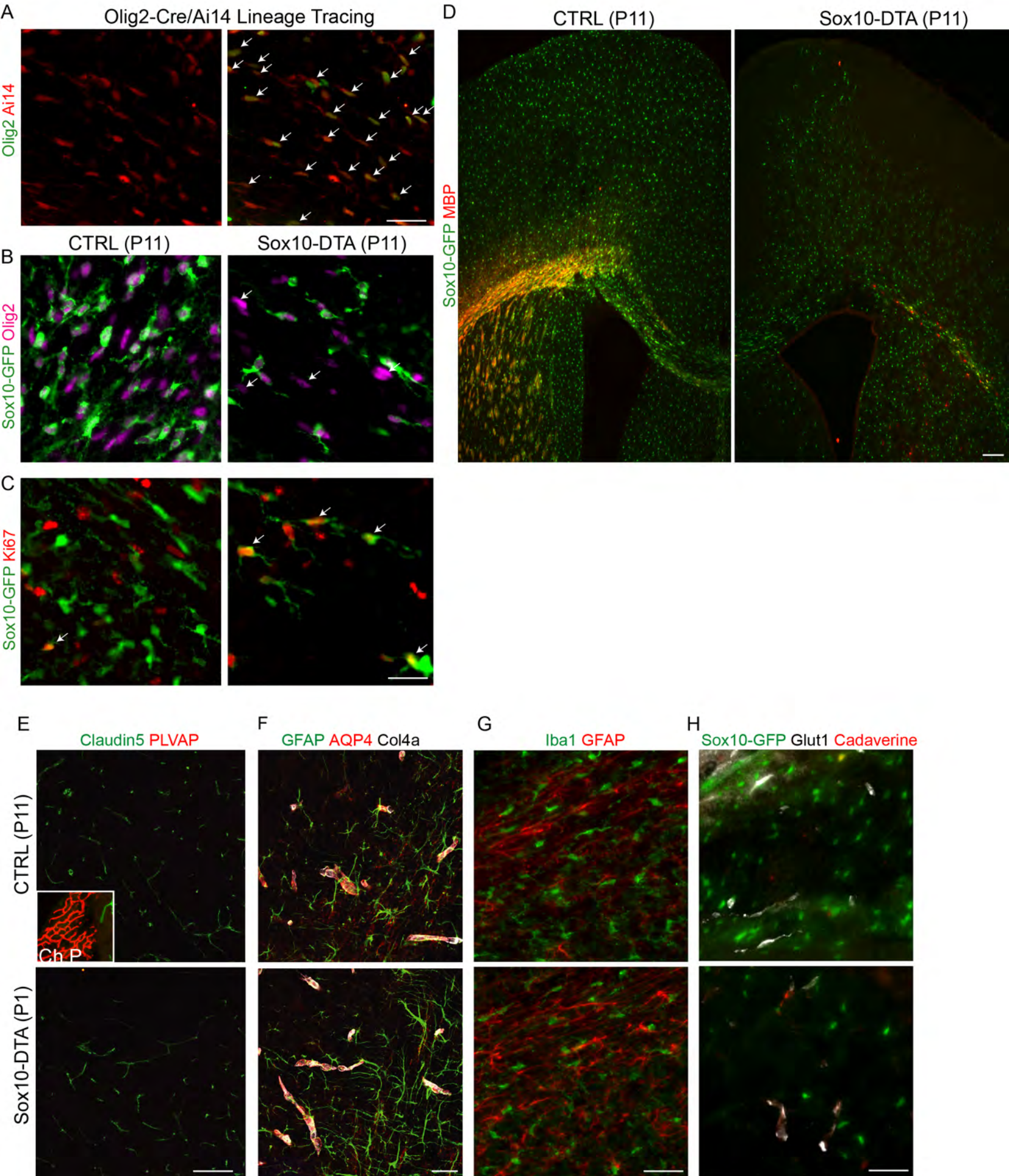

Supplementary Figure 3

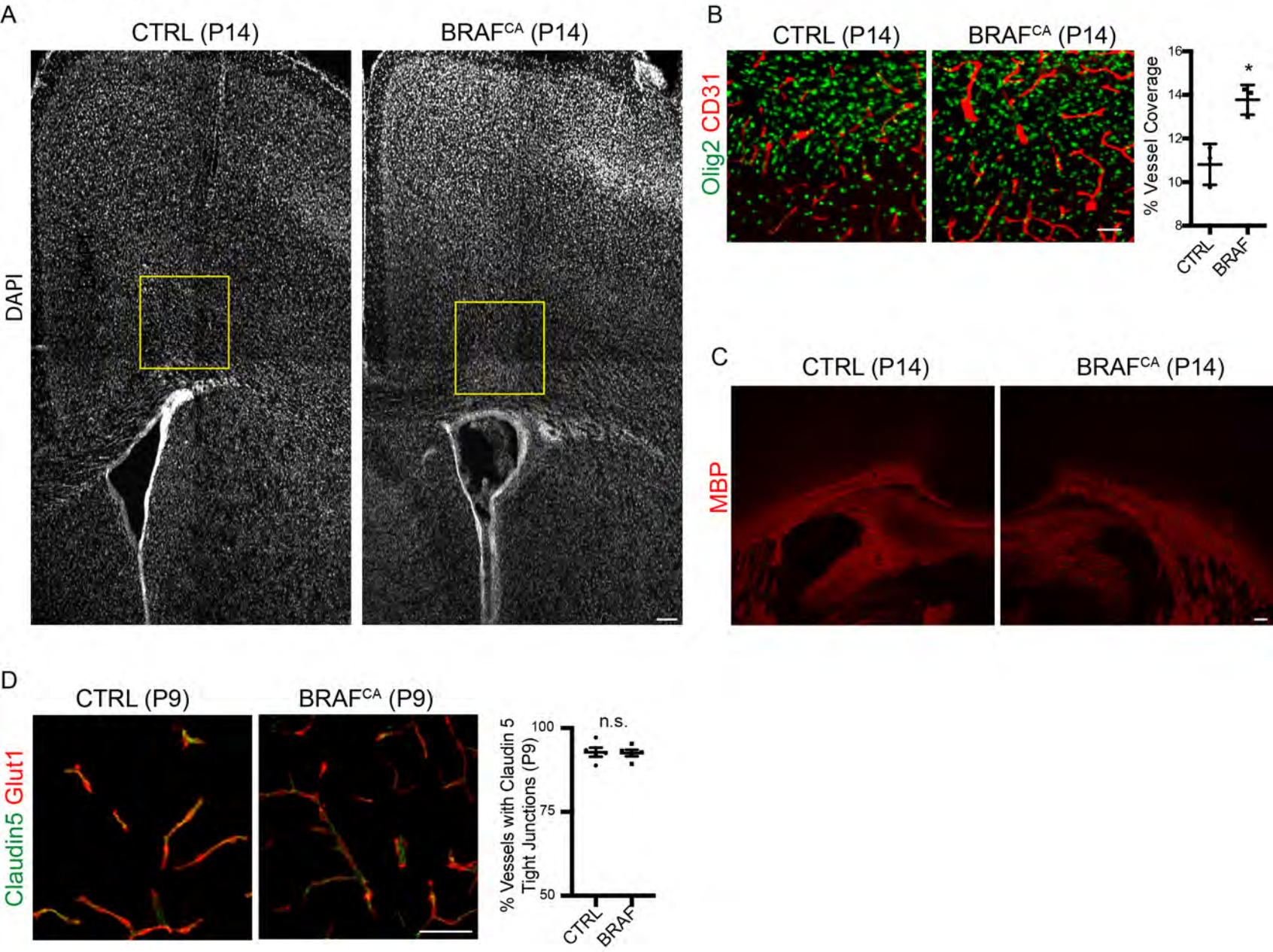

Supplementary Figure 4

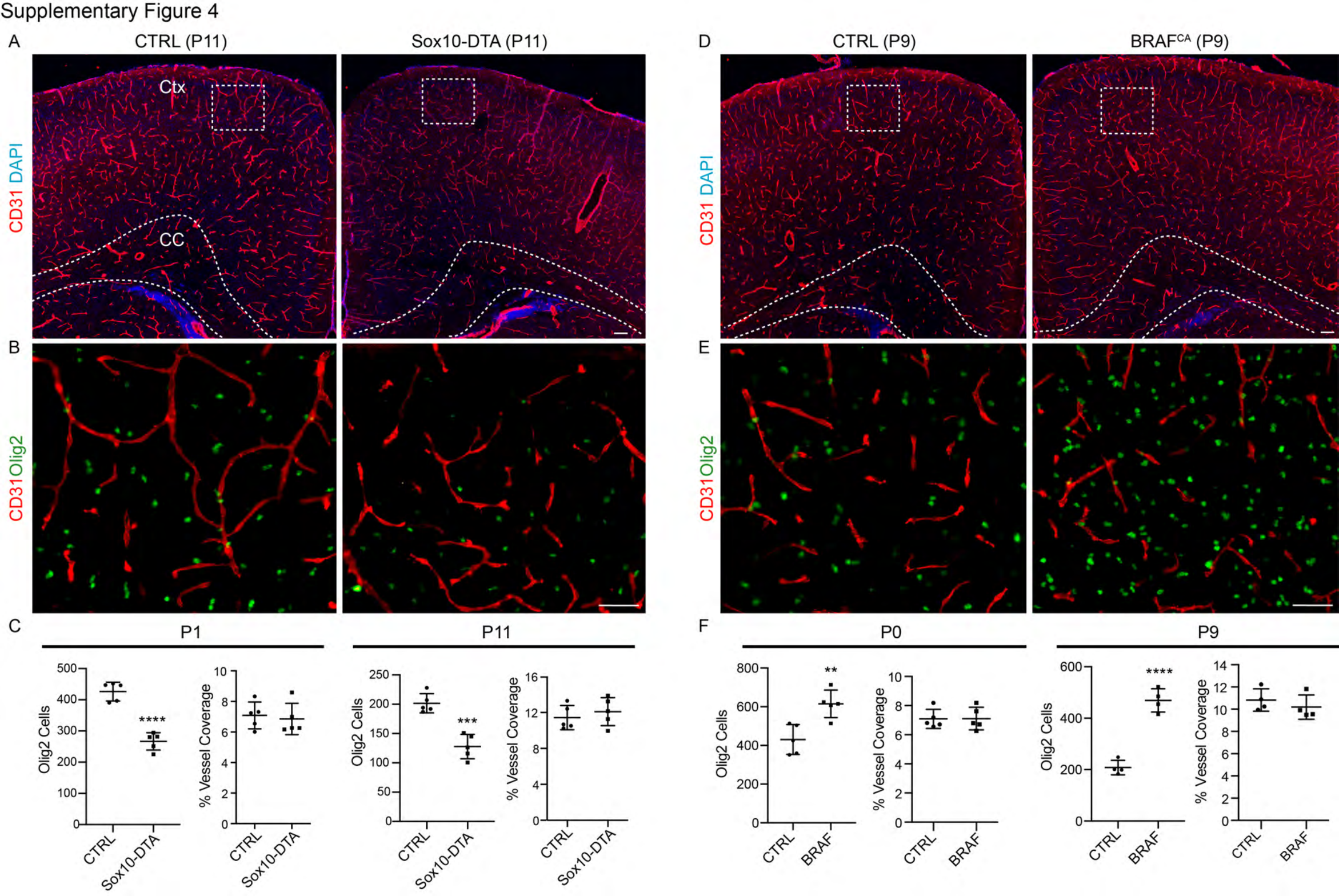

Supplementary Figure 5

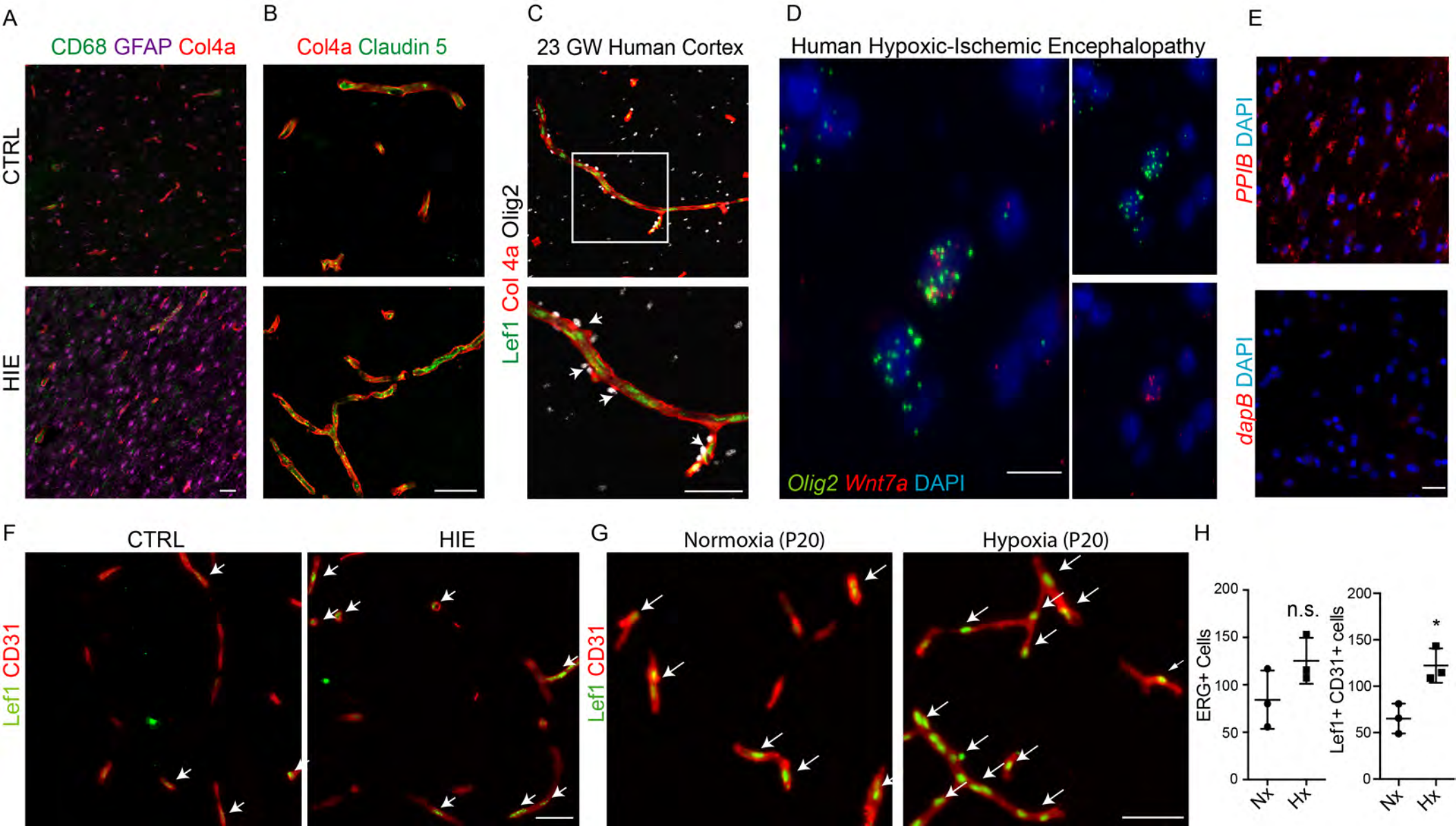

Supplementary Figure 6

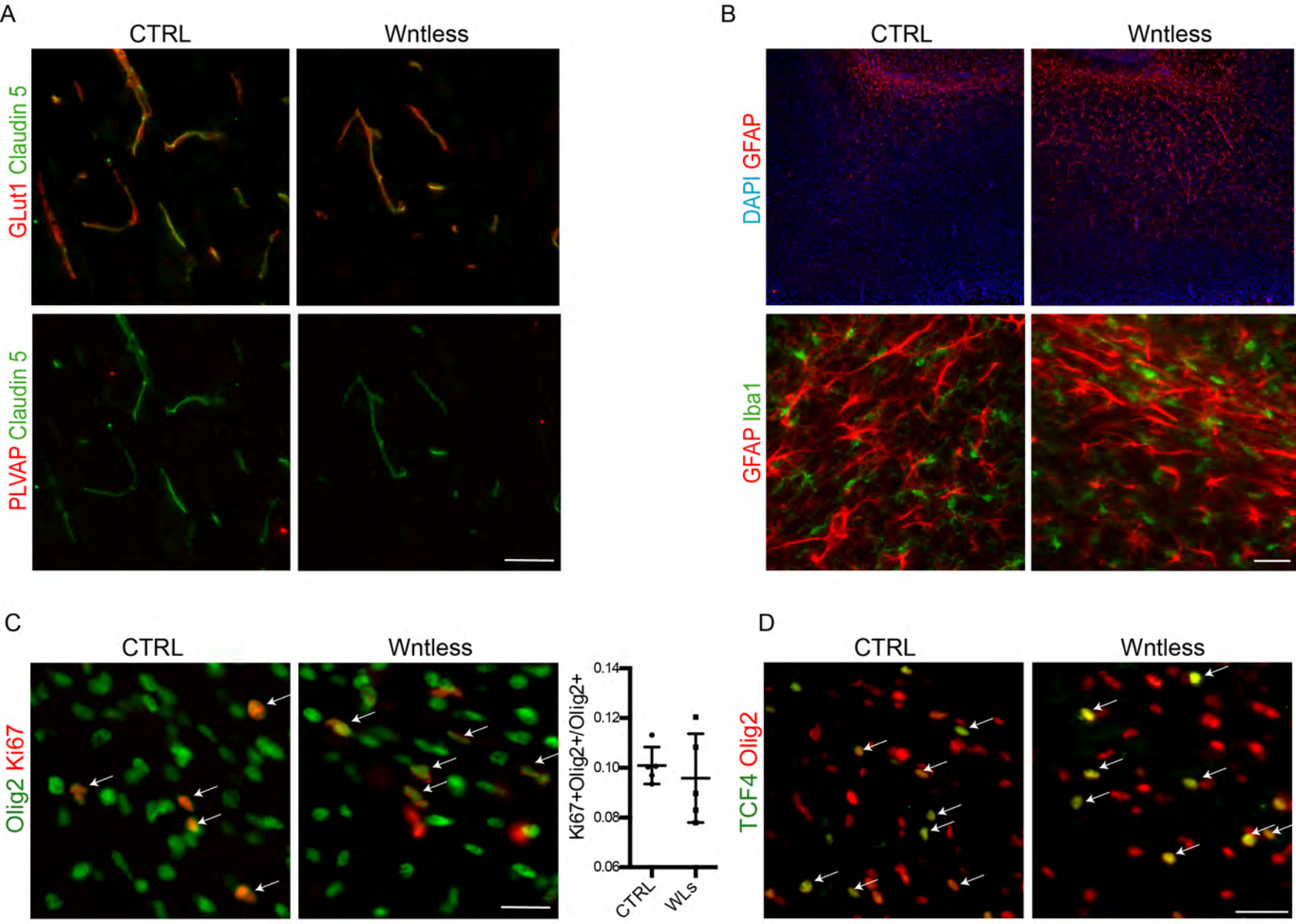

Supplementary Figure 7

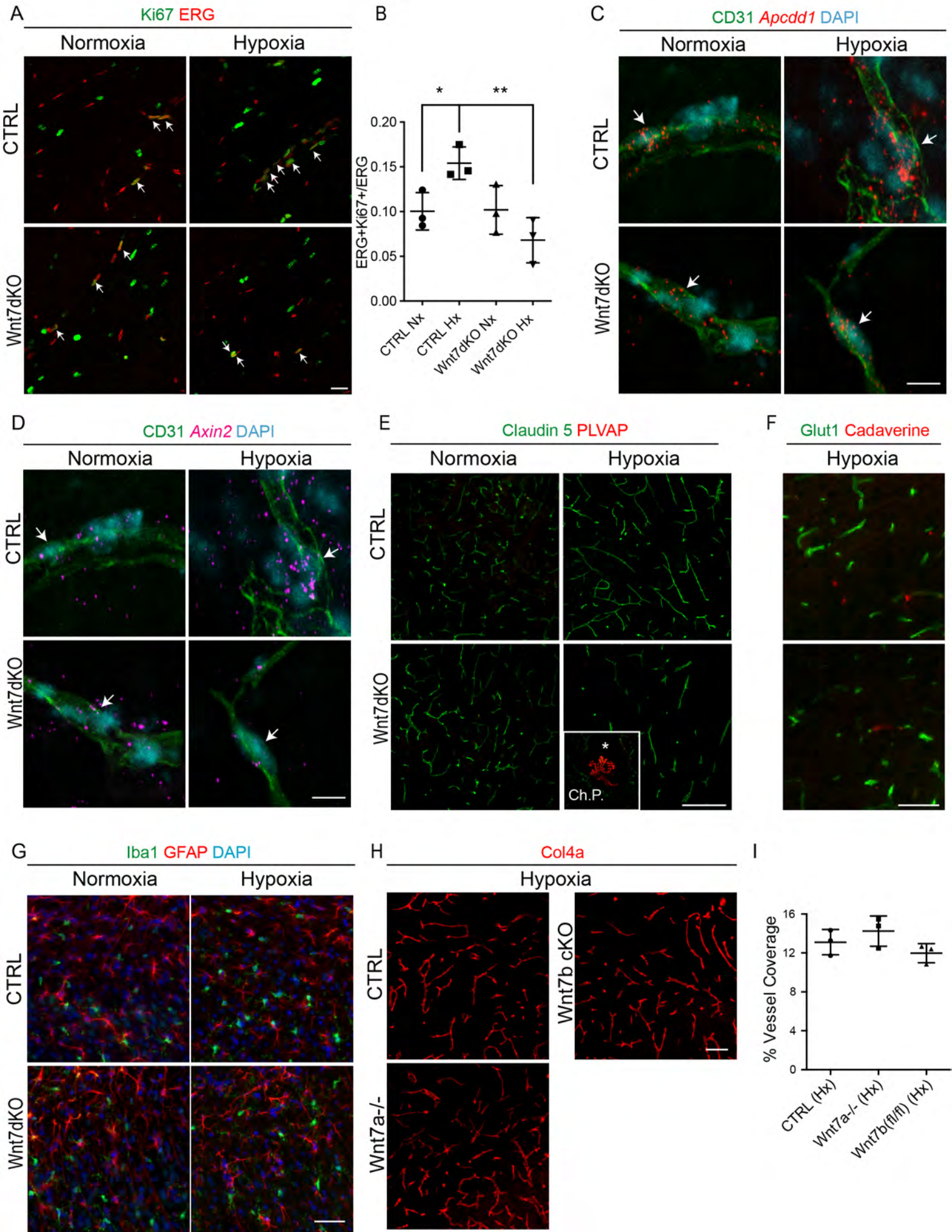

Supplementary Figure 8